Membrane Design for Non-Aqueous Redox Flow Batteries: Current Status and Path Forward

Michelle L. Lehmann[1,2], Landon Tyler[1,2], Ethan C. Self[2], Guang Yang[2], Jagjit Nanda*[2,3], Tomonori Saito*[2]

[1]Bredesen Center for Interdisciplinary Research and Graduate Education, University of Tennessee Knoxville, Knoxville, TN 37966, United States
[2]Chemical Sciences Division, Oak Ridge National Laboratory, Oak Ridge, TN 37831, United States
[3]Department of Chemical Engineering, University of Tennessee Knoxville, Knoxville, TN 37966, United States

Corresponding Authors

*Jagjit Nanda
PO Box 2008, MS6124
Oak Ridge, TN 37831-6124
USA
nandaj@ornl.gov

*Tomonori Saito
PO Box 2008, MS6210
Oak Ridge, TN 37831-6210
USA
saitot@ornl.gov

Abstract

Redox flow batteries are promising technologies for long-duration, large-scale energy storage applications. Among them, non-aqueous redox flow batteries (NARFB) represent a transformative flow battery system since NARFBs potentially offer a higher energy density than aqueous flow batteries. However, many technical challenges remain for NARFBs, including the lack of high-performance membranes, low solubility of redox materials, and poor cycling efficiencies. Membranes serve a vital function in NARFBs, as they allow for selective ion transport while providing separation between the anolyte and catholyte. NARFB membrane development is an emerging research area, and this article reviews their design and critical factors that influence membrane properties, including solvent uptake, ion transport, and redox species permeability. A greater understanding of membrane behavior in non-aqueous solutions provides design principles for developing next-generation membranes for NARFB. Finally, we summarize the challenges, target metrics, and future perspectives for NARFBs.

The Bigger Picture

Many countries have enacted renewable energy targets of 32% or more by 2040 to reduce their carbon footprint. However, due to the intermittent nature of renewable energy sources, stationary energy storage systems are vital for providing a secure and stable electricity supply. Redox flow batteries (RFBs) are well suited for grid storage applications due to their modular design and ability to decouple energy and power. Furthermore, non-aqueous redox flow batteries (NARFBs) show great potential as next-generation RFBs due to their flexible material selection and wide operating voltage window. This review highlights several key challenges and future perspectives of NARFBs, with a focus on membrane development. Understanding membrane design strategies and challenges provides a path forward for the widespread adoption of next-generation RFBs. Moreover, insights into the design principles of membranes for non-aqueous systems lay a strong foundation for the development of electrolyte separators for solid-state batteries and other energy storage systems.

Keywords Redox flow battery, ion exchange membrane, non-aqueous, long-duration energy storage

Introduction

Large-scale, long-duration energy storage (LDES) is a key technology to enable widespread adoption of renewable energy resources (solar, wind, etc.) and to meet the growing demands of an energy intensive economy. Further, increased renewable energy penetration in the electric grid is essential for decarbonization to address global climate change. Several governments and states have mandated targets to increase electricity generation from renewable sources. For example, the European Union set a 32% renewable target by 2035,[1] and California plans to achieve net-zero carbon by 2040.[2] The switch to renewables requires a diverse and flexible energy storage portfolio to meet the power demands of the grid and energy-intensive manufacturing processes. A recent

techno-economic study suggests that for storage between 10-100 hours at rated power, the levelized cost of storage (LCOS) should be ≥ \$0.05 kWh^{-1}.[3] Furthermore, The United States Department of Energy (DOE) long duration storage shot's recent announcement sets an aggressive goal of reducing grid-scale energy cost by 90% within the next decade for systems delivering 10 plus hours of storage.[4] This target is based on the \$162 kWh^{-1} 2020 capital cost of a 100 MW lithium-ion battery. To meet this demand, new battery technologies utilizing earth-abundant and low-cost components are necessary. The majority of energy storage systems on the grid utilize lithium-ion batteries, and redox flow batteries (RFBs) occupy less than 1% of the market.[5] Current Li-ion batteries thrive mainly at shorter durations (less than 4hr), where their value can overcome their high cost. However, the LCOS for Li-ion batteries increases with storage duration.[3] In addition, the use of Li-ion batteries in large-scale installments introduces engineering complexity and safety challenges. For example, a single cell or pack failure can lead to thermal runaway propagating through the entire system.[6] Thus, it is imperative to advance alternative battery chemistries for large-scale stationary applications. RFBs are well suited for LDES due to their modular design and ability to decouple power and energy performance.[7,8]

Non-aqueous RFBs (NARFBs) have emerged as alternatives to aqueous RFBs (Figure 1). The use of an organic solvent can offer a much higher operating voltage than aqueous RFBs, which in turn can increase the system's energy density. NARFBs show great potential as next-generation RFBs, with some systems having theoretical specific energies over 200 Wh kg^{-1}, almost 10 times greater than aqueous vanadium RFBs.[9] A DOE report predicts the LCOS of utility-scale installments for a chromium/iron-based NARFB (\$0.20-0.25 kWh^{-1}) to be half that of an aqueous vanadium RFB (\$0.42-0.48 kWh^{-1}).[10] However, many challenges still need to be addressed before NARFBs can reach commercial viability, including the development of redox-active species with improved stability/solubility and higher performance membranes.

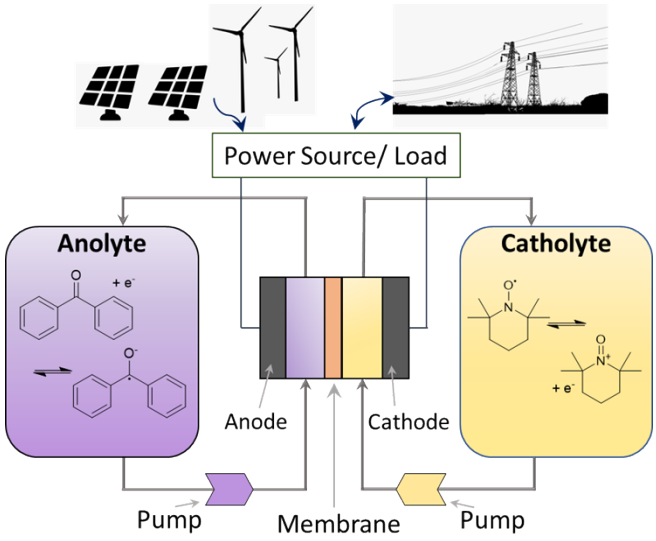

Figure 1. Schematic of a non-aqueous redox flow battery, with examples of organic-based redox couples. Anolyte contains benzophenone (BP), and catholyte contains 2,2,6,6-tetramethyl-1-piperidinyloxy (TEMPO).

To achieve stable NARFB performance, membranes must provide high mechanical strength, high ionic conductivity and selectivity, and excellent chemical and electrochemical stability.[11] The development of membranes designed explicitly for NARFBs has only occurred within the last decade. A recent review by Li et al. summarizes membrane performance and characterization techniques useful for NARFB applications.[12] The most widely used membranes for NARFBs include microporous separators (e.g., Celgard) and polymer membranes originally designed for aqueous systems (e.g., Nafion). Unfortunately, microporous porous separators are unable to prevent anolyte/catholyte crossover, and commercially available membranes for aqueous systems often exhibit poor mechanical and chemical stability in the organic solvents used in NARFBs.

This review is comprised of three parts: (i) a brief overview of redox-active materials and their performance in NARFBs, (ii) a detailed discussion on membrane development, chemistry, and synthesis techniques and how these factors govern membrane performance, and (iii) an in-depth discussion into factors controlling electrolyte uptake, ion transport, and redox species permeability in non-aqueous systems. The effect of organic solvents on membrane properties in non-aqueous systems is complex and not well-understood. Greater insight into the impact of organic solvents on membrane properties will provide design strategies for improved membranes for NARFBs and other battery technologies.

Overview of NARFB Chemistries and Performance

NARFBs allow for the use of a large variety of redox couples, and several comprehensive reviews have been recently published, covering both metal and organic-based redox materials.[7,13] A brief overview of selected redox couple systems is covered here and summarized in Table 1. Metal-ligand-based redox species consist of a transition metal center and ligand. The most widely employed transition metals are iron, cobalt, vanadium, ruthenium, and chromium. Common ligands include acetylacetonate ($M(acac)_3$) and cyclopentadienyl anions (metallocene-type compounds, e.g., ferrocene, Fc) (Figure 2a-b). Metal-ligand-based complexes tend to have low solubility in organic solvents, reducing the energy density of the battery. $M(acac)_3$ redox species (M= Cr, V, Ru) typically have solubilities in the range of 0.05 to 0.1 M in acetonitrile.[14] The solubility of metallocene complexes can be improved by adding functional groups to the cyclopentadienyl rings.[15] For example, the solubility of Fc in a carbonate mixture (ethylene carbonate (EC)/propylene carbonate (PC)/ethyl methyl carbonate (EMC)) increased from 0.04 M to 0.85 M with the addition of a quaternary ammonium group to one of the cyclopentadienyl rings (Figure 3a).[15] With the increase in solubility of the Fc complex, battery performance was reduced at the higher concentration (90% Coulombic efficiency (CE) at 0.8 M compared to 99% CE at 0.01 M). The decrease in efficiency was attributed to increased solution viscosity and the need to utilize

a lower current density (1.5 mA cm^{-2} compared to 3.5 mA cm^{-2}) and highlights the challenges faced with high concentrations of active material.

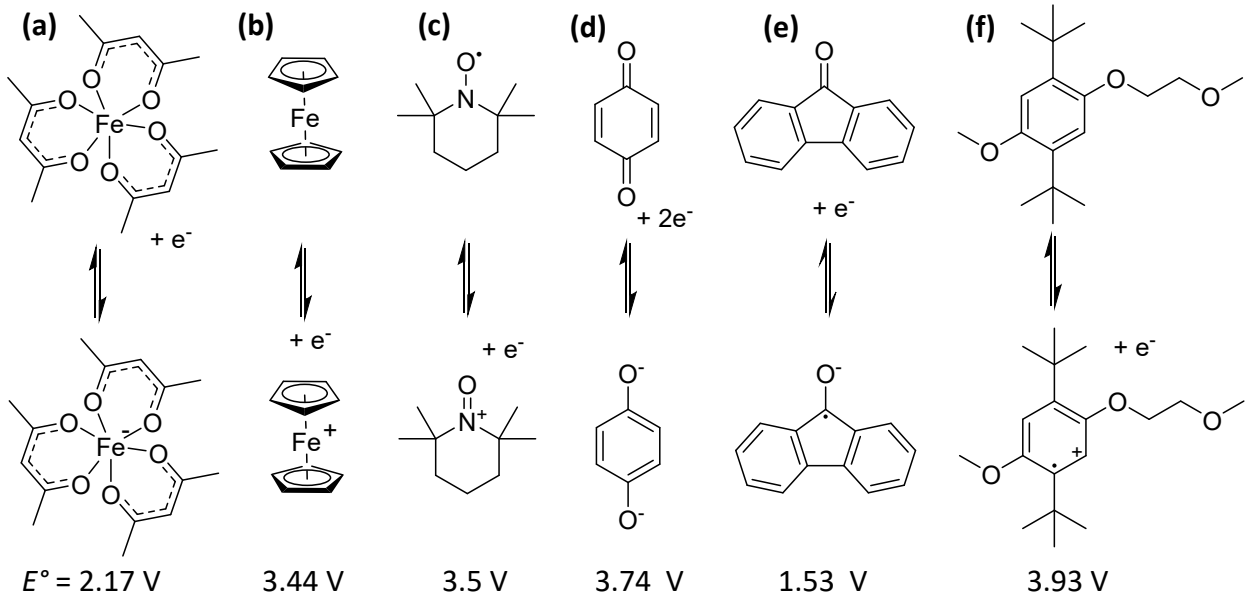

Figure 2. (a-b) Metal-ligand-based and (c-f) organic-based redox-active materials with approximate redox potentials vs. Li/Li^+ (a) Iron acetylacetonate ($Fe(acac)_3$). (b) Ferrocene (Fc). (c) 2,2,6,6-tetramethyl-1-piperidinyloxy (TEMPO). (d) benzoquinone (e) fluorenone (FL). (f) 2,5-di-tert-butyl-1-methoxy-4-[2′-methoxyethoxy]benzene (DBMMB).

Table 1. Summary of several NARFB chemistries and performance.

Redox Couple [a]	Electrolyte	Membrane	Cell Potential (V)[b]	Energy Density (W h L^{-1})[b]	CE/EE[d] (%)	Number of Cycles	Current Density (mA cm^{-2})	Ref
$Fe(acac)_3$| $Cr(acac)_3$	0.4 M $TEABF_4$ in AN/ Dioxane	Nafion + Si nanoparticles (CEM)	1.2	-	99/53	50	5	16
Fc1N112-TFSI| Li	1M LiTFSI in EC/PC/EMC/ FEC	polyethylene based (porous)	3.5	50	90/76	18	1.5	15
15D3GQ |Li	1M $LiPF_6$ in PC	Celgard (porous)	2.4	25	-/70	9	10	17
BP| TEMPO	0.5M $TEAPF_6$ in AN	UltrexTM AMI-7001 (AEM)	2.4	136	81/42	7	0.5	18
MePH| DBMMB	1M LiTFSI in DME	Daramic 175 (porous)	2.3	9	90/68	50	35	19
Me-TEG-DAAQ symmetric	TEATFSI in DME	Nafion (CEM)	2.7	49	96/-	100	2.1	20
PT3|AQ4	1M $TEABF_4$ in AN	Daramic (porous)	2.8	0.75	91/81	10	13.4	21
4 Oxo TEMPO| (1S)-Camphorquinone	1M $TEABF_4$ in PC	Fumasep FAP- PP375 (AEM)	2.1	-	71/80	3	1	22
FL| DBMMB	1M TEATFSI in AN	Daramic (porous)	2.4	13	90/70	100	15	23
BPh|Fc	1 M $LiClO_4$ in TEGDME	Nafion/ PVDF (CEM)	3.0	-	90/56	20	0.025	24

[a] acac= acetylacetonate, Fc1N112-TFSI= ferrocenylmethyl dimethyl ethyl ammonium bis(trifl uoromethanesulfonyl) imide, 15D3GAQ= 1,5-bis(2-(2-(2-methoxyethoxy)ethoxy) ethoxy)anthracene-9,10-dione, BP= benzophenone, TEMPO=2,2,6,6-tetramethyl-1-piperidinyloxy, MePH= N-methylphthalimide, DBMMB= 2,5-di-tert-butyl-1-methoxy-4-[2′-methoxyethoxy]benzene, Me-TEG-DAAQ=1,4-bis((2-(2-(2-methoxyethoxy)ethoxy)ethyl)amino)-anthracene-9,10-dione, PT3= derivative of phenothiazine, AQ4= derivative of anthraquinone, 4 Oxo TEMPO= 4-oxo-2,2,6,6-tetramethyl-1-piperidinyloxy, FL= 9-fluorenone, BPh= biphenyl, Fc= ferrocene, $TEABF_4$= tetraethylammonium tetrafluoroborate, LiTFSI= lithium bis(trifluoromethanesulfonyl)imide, $LiPF_6$= lithium hexafluorophosphate, $TEAPF_6$= tetraethylammonium hexafluorophosphate, TEATFSI= tetraethylammonium bis(trifluoromethanesulfonyl)imide, $LiClO_4$= lithium perchlorate, AN= acetonitrile, EC= ethylene carbonate, PC= propylene carbonate, EMC= ethyl methyl carbonate, FEC= fluoroethylene carbonate, DME= dimethyloxyethane, TEGDME= tetraethylene glycol dimethylether, CEM= cation exchange membrane, AEM= anion exchange membrane. [b]Theoretical Values. [c] Experimental values. [d] CE= Columbic efficiency, EE= energy efficiency, taken at final cycle number.

Organic-based redox-active materials can be easily modified to improve their solubility, redox potential, kinetics, and stability.[25,26] Examples of redox-active organic molecules include 2,2,6,6-tetramethyl-1-piperidinyloxy (TEMPO), quinones, fluorenone (FL), and 2,5-di-tert-butyl-1-methoxy-4-[2′-methoxyethoxy]benzene (DBMMB) (Figure 2c-f). TEMPO is widely studied for both aqueous and non-aqueous RFBs due to the formation of a stable radical species with high solubility. A TEMPO redox species was soluble up to 5.2 M in carbonate solvents and had a redox potential of 3.5V vs. Li/Li^+.[27] Quinones are relatively inexpensive and commercially available carbonyl compounds. Many quinones and their derivatives (such as 1,4-bis(2-methoxyethoxy) anthraquinone shown in Figure 3b) can provide up to two-electron equivalents to achieve a higher energy density at lower active material concentrations.[21]

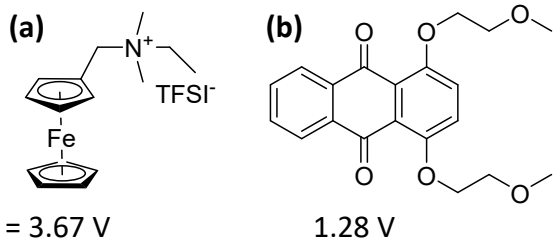

Figure 3. Modified redox-active materials with redox potentials vs. Li/Li^+. (a) Ferrocenylmethyl dimethyl ethyl ammonium bis(trifluoromethanesulfonyl)imide (Fc1N112-TFSI). (b) 1,4-bis(2-methoxyethoxy) anthraquinone (AQ4).

DBMMB is an example of an organic-based active species with a high redox potential (3.93 V vs. Li/Li^+),[28] and when used in conjunction with FL, a flow battery achieved a cell potential of 2.4 V and 90 % CE (Table 1). Furthermore, the stability of radical species formed during cycling was highly dependent on the supporting electrolyte composition (Figure 4).[23] For example, FL exhibited poor stability with the electrolyte TEA-BF_4 (tetraethylammonium tetrafluoroborate) in acetonitrile, while stability greatly improved by changing the salt to TEA-TFSI (tetraethylammonium bis(trifluoromethanesulfonyl)imide) in acetonitrile. In addition to developing anolytes/catholytes with high solubility, another method to increase the energy density of NARBs is to utilize electrochemical reactions.[29,30] Mediated NARFBs have the potential to dramatically increase the energy density of the battery due to the energy being stored in a solid active material rather than the soluble redox species. For example, Self et al. utilized a red phosphorus-based anode mediated by arene anion radical species. The redox-active arenes electrochemically mediated the sodiation/desodiation of the phosphorus to create an anode with a demonstrated solid material capacity of 800 mAh g^{-1}, although parasitic reactions involving the mediators need to be mitigated to improve system lifetime.[9]

Many NARFB studies partially attribute challenges in their battery performance to poor stability and selectivity of the membrane in the system.[19,22] Poor membrane selectivity allows for a significant crossover of the redox species to occur, resulting in low CE. Nevertheless, due to the limited research on membranes designed for NARFBs, performance improvements are mainly

constrained to modifications of the redox-active species. Furthermore, achieving a high current density is important to enable high power density and is directly related to the area specific resistance (ASR) of the electrolyte and separator. The current densities reported for NARFBs with porous separators (10 to 40 mA cm^{-2}) [17,19,23] are generally higher than commercially available dense membranes (0.025 to 2.1 mA cm^{-2}).[20,22,24,31] In comparison, aqueous RFBs operate at much higher current densities on the order of 100 mA cm^{-2}.[32] Thus, to improve battery performance and enable practical current densities, the development of membranes with high ionic conductivity and low permeability is imperative.

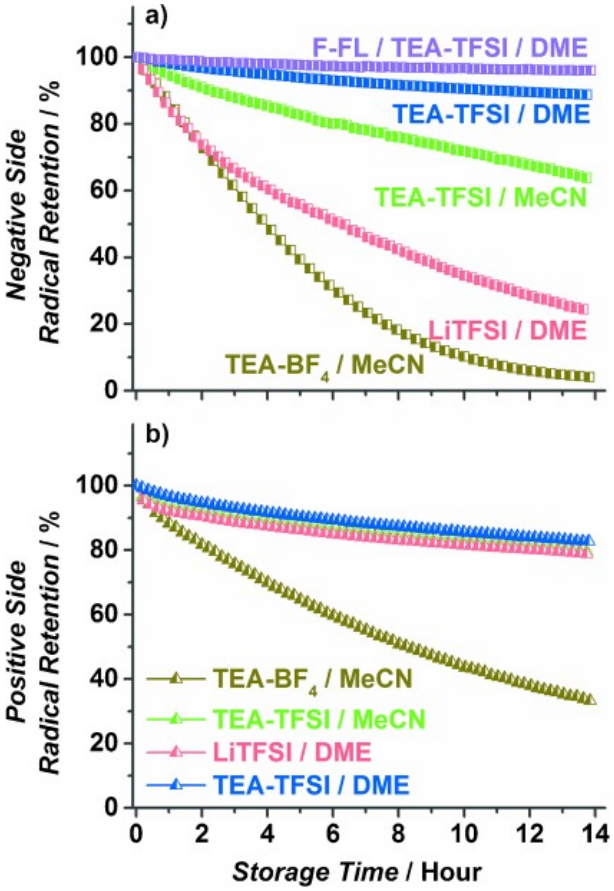

Figure 4. Radical stability in various supporting electrolytes. (a) Negative side ($FL^{\bullet-}$) and (b) positive side ($DBMMB^{\bullet+}$). Reprinted with permission from Wei et al.[23] Copyright 2015 Wiley.

Membranes for NARFB

The US DOE's recent announcement sets an aggressive goal of reducing long-duration energy storage costs by 90% within the next decade. To reach such as aggressive target, achieving enhanced performance while reducing component costs are necessary. Furthermore, next-generation RFBs, such as NARFBs, should be able to achieve a minimum of 1250 cycles, or 5

years of operation, to be competitive with Li-ion systems.[33] Realistically, a lifetime of >10 years is expected. The membrane, as a critical component in a NARFB, should exhibit:

1. *High ionic conductivity*

A membrane needs to have low area specific resistance, which requires thin membranes with high ionic conductivity. Darling et al. recommended a target resistance of < 2.3 Ω cm^2,[33] where for example, 30 μm membrane would require a conductivity of 1.3 mS cm^{-1}.

2. *Low permeability of redox-active species*

Failure to effectively block the transport of the redox-active species through the membrane can lead to self-discharge and irreversible capacity loss. Maintaining a CE of 99.99% or higher is necessary to achieve stable long-term performance of a flow battery. To achieve such high CE of an operating cell, a membrane needs to have an active species permeability of ≤ 10^{-10} cm^2 s^{-1}.

3. *High mechanical stability/ low swelling ratio*

High mechanical and dimensional stability in organic solvents reduces membrane fatigue and enables thinner membranes to be utilized. Excellent mechanical strength also allows the membrane to withstand the pressure induced by flowing liquids in the cell. Excessive dimensional swelling of the membrane reduces its mechanical strength and increases stress when assembled into a device. Furthermore, a membrane with high mechanical strength allows for facile integration into large-scale roll-to-roll manufacturing.

4. *Chemical and electrochemical stability*

Excellent chemical and electrochemical stability mitigate side reactions of the membrane with the electrolyte, which is critical to enable stable device performance. More specifically, the membrane needs to be stable in organic solvents and against highly oxidative and reductive redox couples. Furthermore, to fully utilize the benefits of a non-aqueous system, a wide operating voltage is needed. A simulation study by Chen et al. indicates that many polymers utilized as electrolytes for Li-ion batteries have an electrochemical stability window (ESW) of 4.75 eV.[34] As redox couples are developed that can achieve larger potential windows, the electrochemical stability of the membrane will become a critical factor.

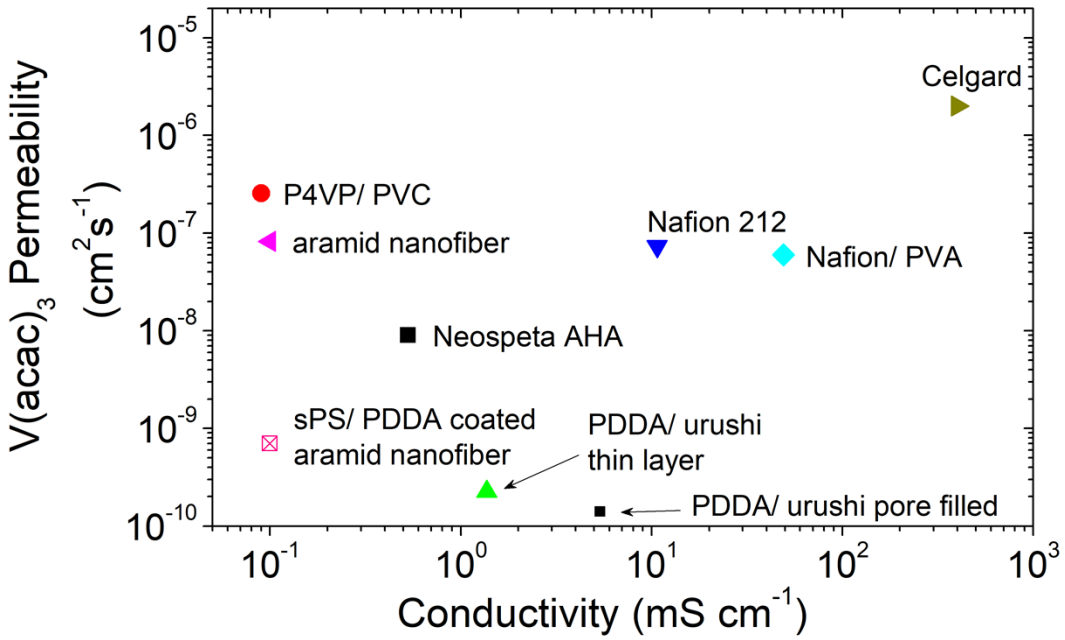

Figure 5. (a) Selectivity of various NARFB membranes. All studies measured the permeability of $V(acac)_3$. References for the data points in the plot are: Celgard, Neosepta AHA, and PDDA/ urushi Ref [35]; P4VP/ PVC, Ref [36]; aramid nanofiber and sPS/ PDDA coated aramid nanofiber, Ref [37]; Nafion/ PVA and Nafion 212, Ref [31]. QPPO= quaternary amine form of poly(phenylene oxide), PDDA= poly(diallyl dimethylammonium), P4VP= poly(4-vinyl pyridine), PVC= polyvinyl chloride, sPS= sulfonated polystyrene, and PVA= polyvinyl alcohol.

Unfortunately, there is often a trade-off among these performance requirements. High ionic conductivity generally comes at the cost of decreased selectivity,[38] as demonstrated with reported values of conductivity and redox species permeability (Figure 5). In addition, many polymeric systems with high mechanical and chemical stability typically exhibit poor room-temperature ionic conductivity.[39-41] For non-aqueous systems, there are many factors involved that impact a membranes' uptake, conductivity, and active species permeability, and these are discussed in detail later in this review. Here, we provide an overview of works developing membranes for NARFBs, with an emphasis on membrane chemistry. For this review, membranes are classified into 4 broad categories: anion exchange membrane (AEM), cation exchange membrane (CEM), porous membrane, and other functional membranes (Figure 6). Other functional membranes are classified here as membranes that contain a combination of exclusion methods, such as a porous anion exchange membrane.

AEMs are the most widely developed membranes for NARFBs. The cation tethered to the polymer backbone aids the transport of an anion while blocking the transport of positively charged species by Donnan exclusion. Many redox couples are positively charged (e.g., ferrocenium cation), with the charge carrier being the anion. Thus, AEMs can serve as the appropriate choice of membrane

for these systems. On the other hand, CEMs contain an anion tethered to the polymer backbone, allowing the transport of cations through the membrane while blocking the transport of anions. Porous membranes are defined here as separators that do not contain any chemical functionality to inhibit the transport of redox couples or ions. Porous separators block the transport of redox species via size exclusion, though often, the pore size is larger than the solvated redox compound. Porous separators allow for transport of both anion and cation, thus offering no selectivity toward the charge carrier. Other functional membranes, as defined here, are porous membranes with added chemical functionality to block the transport of redox species via size exclusion and Donnan exclusion.

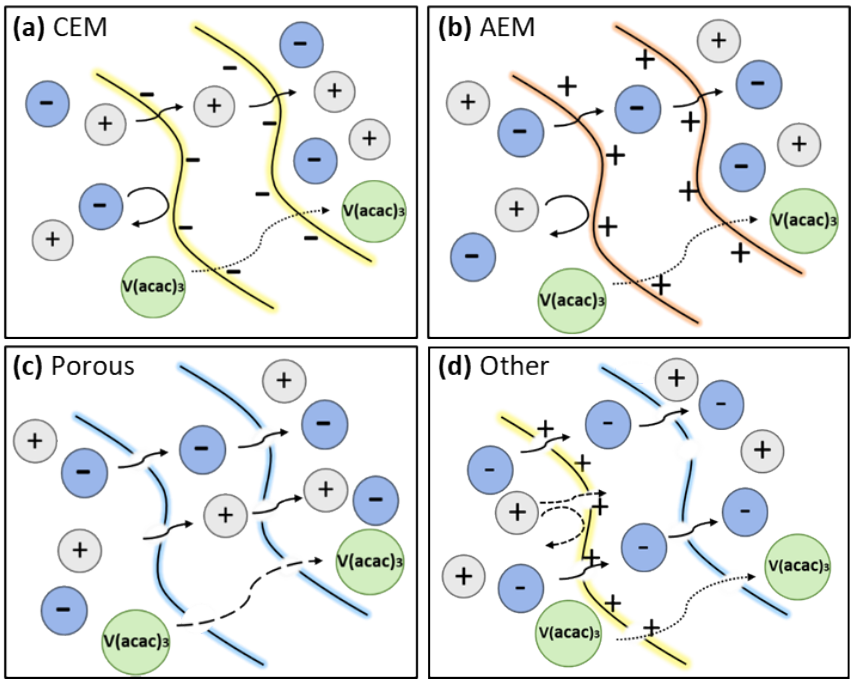

Figure 6. Schematic of the 4 categories of membranes for NARFBs and their ion transport mechanism. (a) Cation exchange membrane, (b) anion exchange membrane, (c) porous separator, and (d) other functional membranes. The arrows represent the relative ease of ion transport through the membrane: solid fast transport, dash moderate transport, and dotted slow transport.

To date, a handful of ionic groups have been utilized for ion exchange membranes for NARFBs (see Figure 7a and Table 2). In some cases, membranes containing larger cations (i.e., 1-methylpyridinium) exhibit lower $V(acac)_3$ permeability than those prepared with a smaller cation (i.e., trimethylammonium).[42] Examples of potential ionic groups yet to be explored for NARFB membranes are given in Figures 7b and 7c. While the list of ionic groups in Figures 7b and 7c is by no means comprehensive, the depicted cations demonstrate improved stability in aqueous environments, while the anions show improved conductivity lithium-based battery studies.

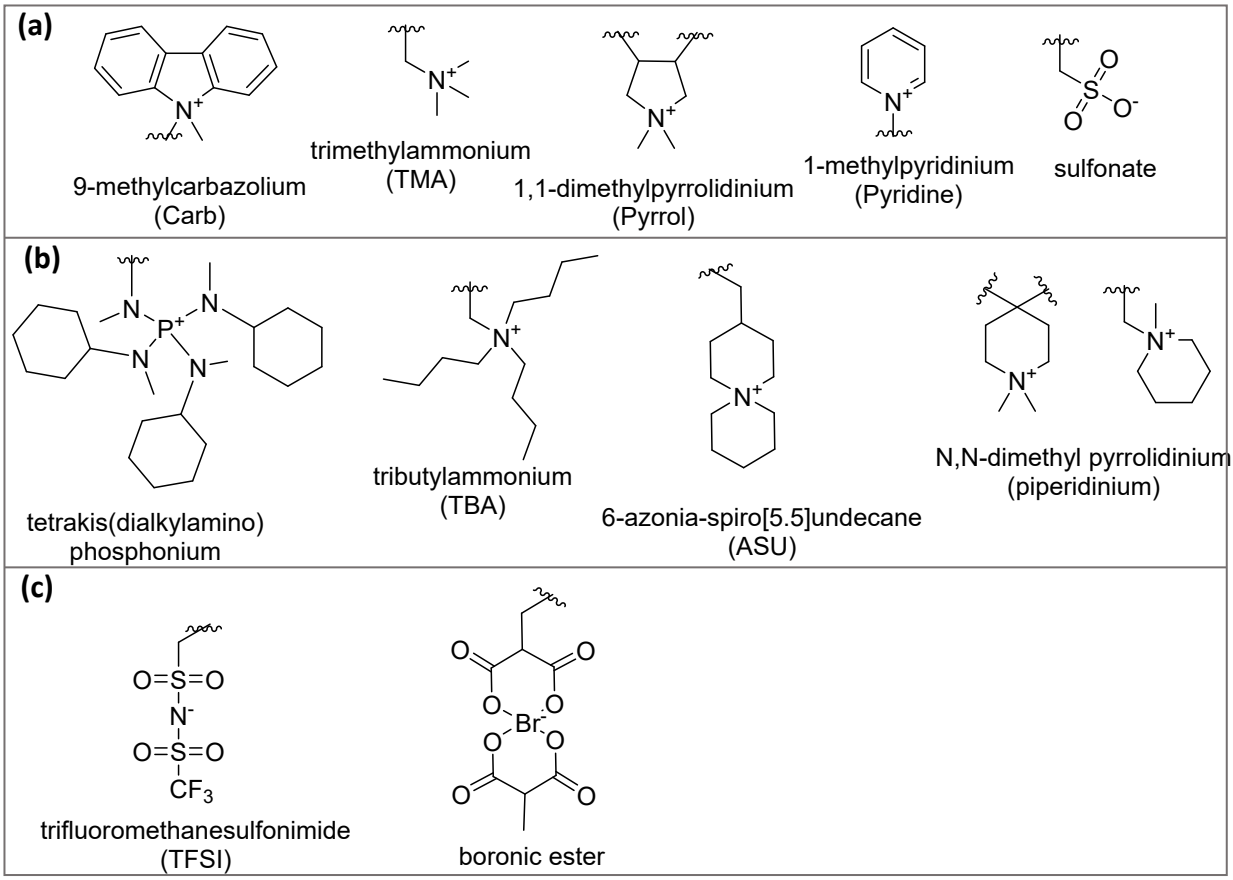

Figure 7. (a) Ionic groups utilized in NARFB membrane studies. For ease of comparison, the abbreviation in parenthesis is the same as that used in Table 2. (b) Examples of potential cationic groups for anion exchange membranes. (c) Examples of potential anionic groups for cation exchange membranes.

Table 2. Summary of NARFB membrane properties.

Membrane	Thickness (μm)	Type/ IEC [a]	Ionic group	Electrolyte	Uptake (%)	Swelling Ratio (%)	Conductivity (mS cm^{-1})	Permeability[b] (cm^2 s^{-1}) ×10^{-7}	Ref
Neosepta AHA	220	AEM 1.39	TMA	0.1M $TEABF_4$ in AN	27	3.5	0.53 - 5.27	0.085 - 0.0957	31,43
Neosepta AHA	220	AEM 1.39	TMA	0.1M $TBABF_4$ in AN	27		0.020	0.03	37
Fumasep FAP-450	55	AEM 0.76	TMA	0.5M $TEABF_4$ in PC	47 - 48		0.481 - 3.46	0.0613 - 0.0976	35,44
PS/DVB on porous support	28	AEM 2.04	TMA	0.5M $TEABF_4$ in PC	10.1		0.430	0.0445	44
PDDA/ Urushi on Celgard	30	AEM	Pyrrol	0.5M $TEABF_4$ in PC	0		1.37	0.00226	35
PGMA with Si/ PVDF	39	AEM 1.55	TMA	1M $TEABF_4$ in AN	35.9	8.9	0.33	83.5	42
P4VP with Si/ PVDF	45	AEM 1.12	pyridine	1M $TEABF_4$ in AN	33.0	9.0	0.39	69.2	42
P4VP with PVC	32	AEM 1.85	pyridine	0.1M $TEABF_4$ in AN	n/a	3.0	0.090	2.56	36
Nafion 212	50	CEM 0.93	sulfonate	0.1M $TEABF_4$ in AN	17.1	9.3	10.7	0.733	31
Nafion 212	55	CEM 0.93	sulfonate	0.5M $TEABF_4$ in PC	38		3.75	0.778	35
Celgard	25	porous	none	0.1M $TEABF_4$ in AN	111		370 - 550	18.4 - 24.0	35,43
W-Scope PE	18	porous	none	1.0M $TEABF_4$ in AN	152	0	4.1	898	42
Aramid nanofiber	8.5	porous	none	0.1M $TBABF_4$ in AN			0.10	0.820	37
sPS/PDDA aramid nanofiber	~12	AEM/ CEM	sulfonate / Pyrrol	0.1M $TBABF_4$ in AN			0.10	0.007	37
PNVC with Si/ PVDF	60	porous / AEM	Carb	0.1M $TBABF_4$ in AN	55.3	9.4	10.1	2150	42
PDDA/ Urushi pore filled Celgard	28	porous / AEM	Pyrrol	0.5M $TEABF_4$ in PC	0		5.37	0.00141	35
PVA/Nafion on Celgard	60	porous / CEM	sulfonate	0.1M $TEABF_4$ in AN	80	0.6	49.1	0.600	31
POATS-PPO	n/a	CEM 1.17	sulfonate	1M LiFSI in DMC	38		0.06	0.03[c]	45

PDDA= poly(diallyl dimethylammonium), PGMA= poly(glycidyl methacrylate), PVDF= polyvinylidene fluoride, P4VP= poly(4-vinyl pyridine), PVC= poly(vinyl chloride), sPS= sulfonated polystyrene, PNVC= poly(N-vinyl carbazole), PVA= poly(vinyl alcohol), TMA= trimethylammonium, Pyrrol = 1,1-dimethylpyrrolidinium, Pyridine= 1-methylpyridinium, Carb= 9-methylcarbazolium, $TEABF_4$= tetraethylammonium tetrafluoroborate, $TBABF_4$= tetrabutylammonium tetrafluoroborate, AN= acetonitrile, PC= propylene carbonate.

[a] IEC = ion exchange capacity of the membrane, defined as the mmoles of ionic units per gram of polymer (meq g^{-1}), [b]Permeability of vanadium acetylacetonate ($V(acac)_3$). [c]Ferrocene permeability. CEM= cation exchange membrane, AEM= anion exchange membrane.

Anion Exchange Membranes (AEMs)

Commercially available AEMs that have been tested in NARFBs include Neosepta AHA and Fumasep FAP membranes. Neosepta AHA is a thick reinforced membrane (220 μm) consisting of a crosslinked styrene-divinylbenzene backbone with an ion exchange capacity (IEC) of 1.39 meq g^{-1}. The membrane demonstrates reasonable BF_4^- conductivity (0.53-5.27 mS cm^{-1}), and $V(acac)_3$ permeability (8.5×10^{-9} to 9.57×10^{-9} cm^2 s^{-1}) performance (Table 2).[31,43] While the ionic conductivity is competitive with other dense membranes, the thickness of the membrane leads to high ASR values (4.1 to 41 Ω cm^2), making it unsuitable for use in high power NARFBs. Using a similar chemical structure as Neosepta AHA, Kim et al. created a pore-filled AEM of only a 28 μm thickness and a higher IEC (2.04 meq g^{-1}) (Figure 8a).[44] The crosslinked styrene-divinylbenzene-benzyl trimethyl ammonium membrane exhibited similar conductivity and permeability values as Neosepta AHA. With the significant reduction in membrane thickness, the ASR was reduced to 0.286 Ω cm^2. Fumasep FAP-450 membranes consist of an unreinforced fluorinated polymer backbone with a low IEC (0.7 meq g^{-1}) and a moderate thickness (50 μm). The FAP-450 membrane demonstrated similar conductivity and permeability values as Neosepta AHA, even with the 4× decrease in membrane thickness (Table 2).

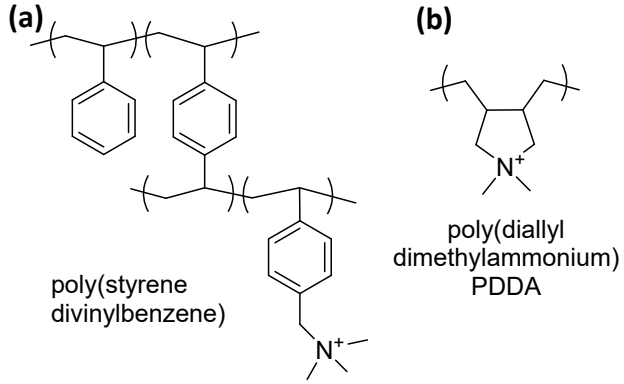

Figure 8. Structure of various polymers used as anion exchange membranes.

An urushi/poly(diallyl dimethylammonium chloride) (PDDA) composite membrane containing 40 wt% PDDA (Figures 8b and 9b) exhibited a $V(acac)_3$ permeability of 2.26×10^{-10} cm^2 s^{-1} and a BF_4^- conductivity of 1.37 mS cm^{-1} (Table 2).[35] The theoretical IEC of the PDDA/urushi polymer was 2.47 meq g^{-1}, though the authors did not report an experimental IEC value. In addition, the cation in PDDA, a 5 membered heterocyclic quaternary ammonium, offers excellent stability in a fuel cell environment,[46] and may also prove to be a suitable choice for NARFBs.

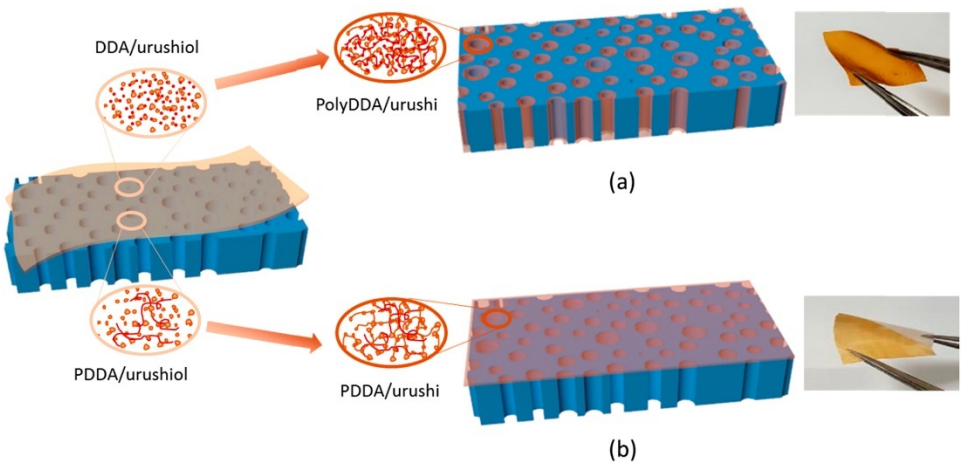

Figure 9. Illustration for the fabrication of an anion exchange membrane consisting of crosslinked poly(diallyl dimethylammonium chloride) (PDDA)/urushi on a Celgard support layer. (a) As a pore-filled membrane (see discussion in Other Functional Membranes) and (b) a thin polymer layer. Reprinted with permission from Kim et al.[35] Copyright 2018 Elsevier.

Shin et al. explored the performance of poly(glycidyl methacrylate) (PGMA)/alkyl trimethyl ammonium and poly(4-vinyl pyridine) (P4VP)/pyridinium (Figures 10a and 10b, respectively) crosslinked polymers with a polyvinylidene fluoride (PVDF) support matrix and silica nanoparticles.[42] PVDF provides a strong chemically inert support, while silica nanoparticles provide additional mechanical strength and reduce the permeability of redox species.[47] The BF_4^- conductivities of these membranes were similar (~0.3 mS cm^{-1}), while the P4VP polymer exhibited a slightly lower $V(acac)_3$ permeability (6.92×10^{-6} vs. 8.35×10^{-6} cm^2 s^{-1} for the PGMA-based membrane, Table 2). The decrease in permeability for P4VP may be attributed to the membrane's higher anion transport number (see transport number discussion below).

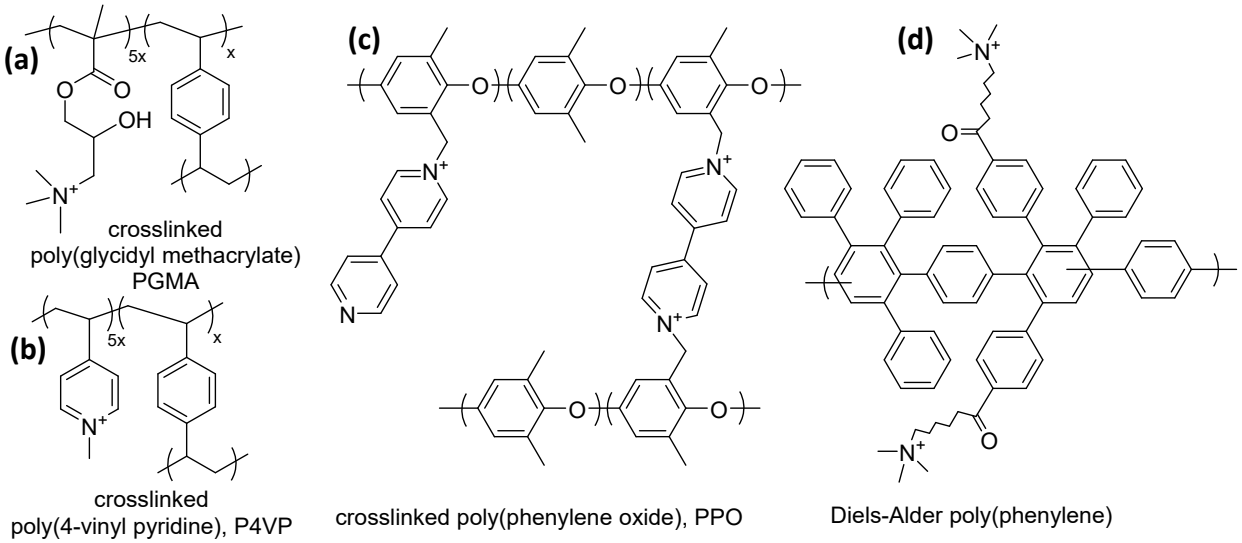

Figure 10. Chemical structure of various anion exchange membranes.

Freestanding membranes consisting of crosslinked poly(phenylene oxide) (PPO) and Diels-Alder polyphenylene have also been studied as separators for NARFBs. Crosslinked PPO membranes (Figure 10c) of varying crosslink densities were prepared by the addition of 4,4′-bipyridine at different molar ratios to brominated PPO.[48] IEC increases with increasing addition of 4, 4′-bipyridine, up to an IEC of 1.03 meq g^{-1}. However, the highest IEC membrane was too brittle for testing. Membranes with an IEC of 0.89 meq g^{-1} had a $[Tf_2N]^-$ conductivity of 0.34 mS cm^{-1} in an AN-based electrolyte with an uptake of 27%. Diels-Alder polyphenylenes consist of a fully aromatic backbone (Figure 10d), which offers improved chemical stability compared to heteroatom containing backbones,[49,50] but also requires a certain amount of electrolyte uptake to soften the backbone to ensure a usable membrane. In a propylene carbonate (PC) based electrolyte, Diels-alder polyphenylene AEMs with IEC values of 2.0 and 2.5 meq g^{-1} exhibited dimensional swelling of 35-40%.[51] These membranes could be tested due to the plasticizing effect of PC, while the membrane with an IEC of 1.5 meq g^{-1} was too brittle and unable to be tested, presumably due to low PC uptake. As expected, BF_4^- conductivity increased with increasing IEC (1.63 to 1.96 mS cm^{-1} for the 2.0 and 2.5 meq g^{-1} IEC membranes, respectively), while CE decreased. A decrease in CE is an indication of increased permeability of the redox species.

Cation Exchange Membranes (CEM)

Nafion® is a commercially available membrane widely studied for proton exchange membrane fuel cells[52] and aqueous vanadium RFBs.[53] Nafion® is a perfluorinated polymer with a sulfonic acid ionic group and is available in a variety of thicknesses, with or without a support matrix (Figure 11). Nafion's chemical structure can form a phase separated morphology that provides ion-conducting channels, leading to high proton conductivity (60-90 mS cm^{-1}) in aqueous systems.[54,55] When used in non-aqueous media, proton conductivity is significantly decreased (3.6 mS cm^{-1} in dimethyl sulfoxide (DMSO)).[56] Permeability of neutral $V(acac)_3$ through Nafion is relatively high compared to the commercial AEMs of Neosepta and Fumasep (Table 2). [31,35,44] Despite the moderate redox species crossover through Nafion, few reports exist on the development of alternative CEMs for NARFBs. McCormack et al. synthesized a PPO membrane with an ionic phenoxyaniline tri-sulfonate side chain (Figure 12).[45] In an electrolyte solution containing 1M LiTFSI in dimethyl carbonate (DMC), the conductivity increased with the membrane's IEC, while permeability of Fc remained relatively constant. While Fc permeability was higher for the PPO membranes (~3.5×10^{-9} cm^2 s^{-1}, Table 2) than that of Nafion (~6.0×10^{-11} cm^2 s^{-1}), electrolyte uptake and Li^+ conductivity of Nafion was significantly lower. The PPO membrane with the lowest IEC (0.75 meq g^{-1}) exhibited a conductivity of 0.015 mS cm^{-1}, while the membrane with the highest IEC (1.17 meq g^{-1}) had a conductivity of 0.6 mS cm^{-1}.

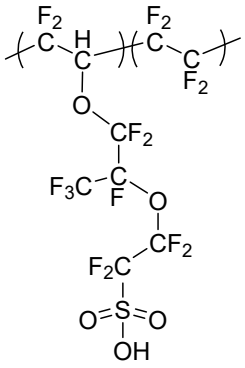

Figure 11. Chemical structure of Nafion.

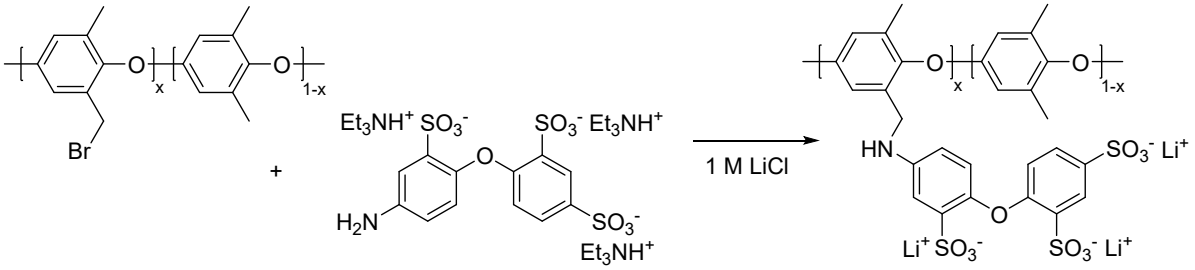

Figure 12. Synthesis scheme for the fabrication of a Li-ion conducting poly(phenylene oxide) membrane. Modified and reprinted with permission from McCormack et al.[45] Copyright 2020 Elsevier.

Porous Membranes

Commercially available porous separators such as Celgard have been widely used in NARFBs due to their good wettability, low cost, and chemical stability.[57] The average pore size of Celgard is approximately 28 nm but can contain pores as large as 40 μm,[25,37,57] while the size of redox species such as $V(acac)_3$ is < 1 nm.[31] The porous structure enables high ionic conductivity (Table 2) but also results in high $V(acac)_3$ permeability ca. 2×10^{-6} cm^2 s^{-1}.[43] As a side note, a large discrepancy was found in the conductivity values reported for the liquid electrolyte 0.1 M $TEABF_4$/AN without Celgard and 0.1 M $TEABF_4$/AN with Celgard from NARFB membrane studies, shown in Table 2. Reported conductivity values of the liquid 0.1 M $TEABF_4$/AN electrolyte are 11 to 55 mS cm^{-1},[58,59] while those in Table 2 reported 370 to 550 mS cm^{-1}, an order of magnitude larger. The addition of Celgard should decrease the conductivity of the liquid electrolyte. The difference may be due to the measurement techniques and/or reagent purity used, but indicates that conductivity values alone are not a good determining factor of membrane performance. A nanoporous separator consisting of aramid nanofibers with a pore size of 5 nm demonstrated improved blocking of $V(acac)_3$ permeability compared to Celgard.[37] The permeability rate was 8.2×10^{-8} cm^2 s^{-1}, 2-orders lower than Celgard, though at the expense of a significantly reduced BF_4^- conductivity (0.1 mS cm^{-1}) (Table 2). The performance of porous membranes may be enhanced with the addition of chemical functionality to the membrane surface or within the pores of the membrane.

Other Functional Membranes

Several studies have utilized membranes that cannot be categorized solely into one of the groups mentioned above, such as porous membranes that also include anion exchange functionality. One study fabricated a PDDA/urushi pore-filled membrane via in-situ polymerization of monomers within the pores of a Celgard separator (Figure 9a).[35] This method reduced the pore volume of neat Celgard by ~20×. $V(acac)_3$ permeability of the charged porous membrane decreased by 1.6× compared to a thin PDDA/urushi layer coated onto Celgard, without a reduction in conductivity (Table 2). In another system, a porous AEM (average pore size of 607 nm) was fabricated from a bulky poly(N-vinyl carbazole) (PNVC) polymeric structure (Figure 13) and a PVDF support.[42] The authors attribute the formation of the larger than expected pores to the low compatibility between PNVC and PVDF, resulting in cavity formation. The porous structure resulted in a significant increase in the permeability of $V(acac)_3$ compared to Celgard, even with the presence of additional functionality (Table 2). Another example of a porous AEM consists of electrospun Nafion-based fibers on a Celgard support.[31] The porous selective layer was fabricated by electrospinning a 2:1 molar ratio of poly(vinyl alcohol) (PVA) and Nafion. The selective layer was 35 μm thick, and the conductivity of the porous membrane was 5× higher than that of a dense Nafion membrane while maintaining a similar permeability (Table 2).

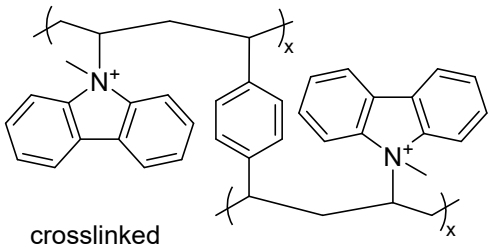

Figure 13. Structure of polymer used as a porous anion exchange membrane.

Impact of Non-Aqueous Solutions on Membrane Properties

To design membranes for NARFBs, it is imperative to establish an understanding of the structure-property relationships and the dynamics of ion transport in non-aqueous systems.[56,60] Considering the vast combination of supporting electrolytes and redox-active species possible for NARFBs, developing correlations between the supporting electrolyte composition and membrane properties (i.e., uptake, ion transport, permeability) is imperative for developing high-performance NARFB membranes.

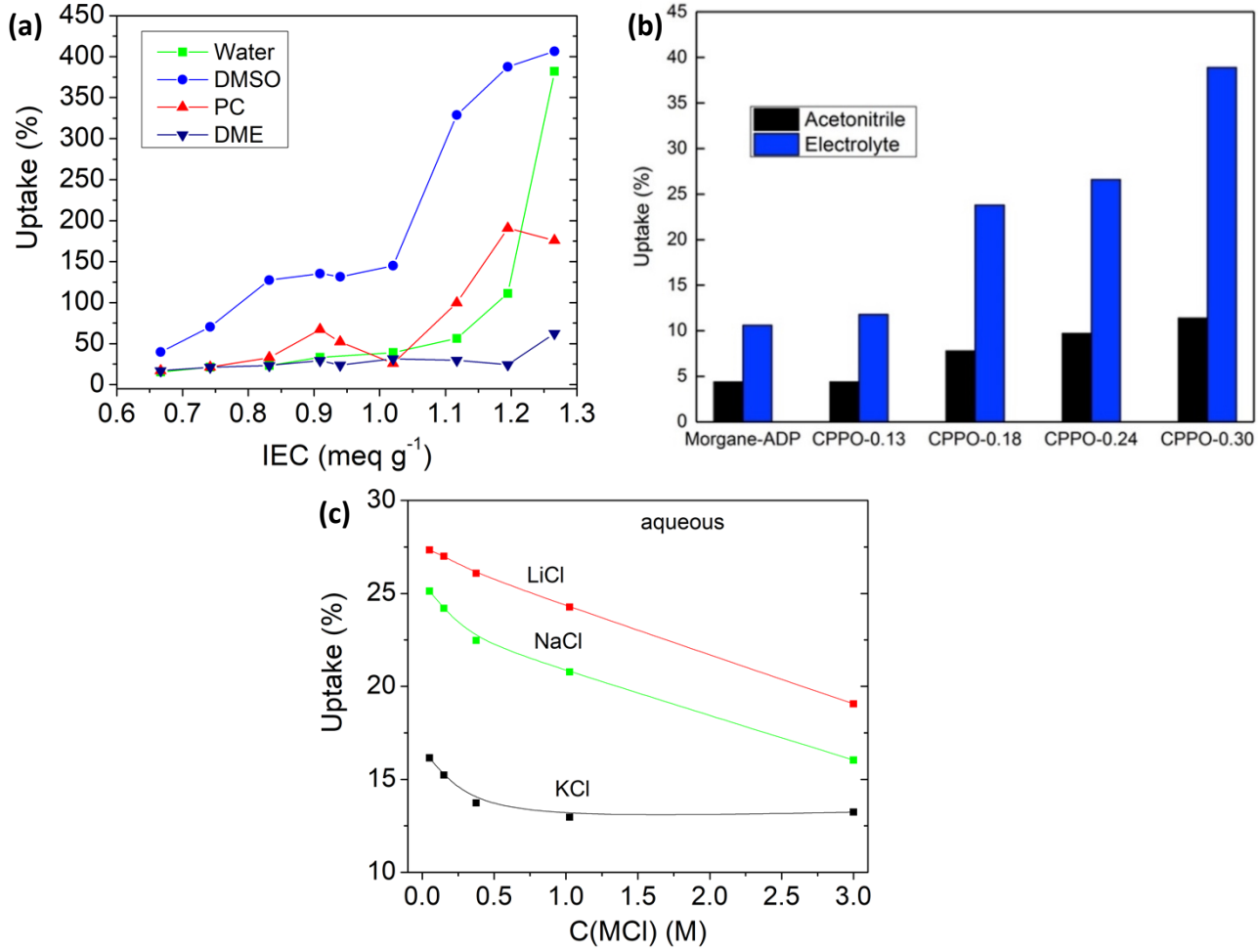

Figure 14. (a) Solvent uptake versus IEC of Li-Nafion in various solvents. Modified and reprinted with permission from Doyle et al.[61] Copyright 2001 American Chemical Society. (b) Uptake of crosslinked poly(phenylene oxide) (PPO) anion exchange membranes of various IECs (0.49, 0.87, 0.89, 1.03) in AN and electrolyte solution. Reprinted with permission from Li et al.[48] Copyright 2018 Elsevier. (c) Uptake of Nafion-117 equilibrated in various concentrations of aqueous salt solutions. Modified and reprinted with permission from Stenina et al.[62] Copyright 2004 Elsevier.

Solvent Uptake.

It is essential to control a membrane's electrolyte uptake and swelling in flow battery applications. A large amount of solvent uptake generally increases ionic conductivity, but excessive uptake results in high permeability and loss of mechanical integrity. On the other hand, when the uptake is limited, the membrane typically exhibits poor ionic conductivity. Uptake is generally correlated with membrane dimensional swelling unless a support layer is utilized (see discussion below). In aqueous solutions, backbone flexibility,[63,64] polarity,[65,66] and membrane IEC[67,68] have a significant impact on electrolyte uptake. Due to the ionic groups being hydrophilic, water uptake increases

with higher IEC in aqueous systems; thus, there is a balance between ionic conductivity and swelling of the membrane. In non-aqueous solutions, the relationship is much more complex. Solvent uptake is affected by the physical properties of the polymer as well as that of the solvent.

The effect of solvent properties on lithiated Nafion (Li-Nafion) uptake has been comprehensively studied by Doyle et al.[56] In general, solvent uptake increased with donor number and dielectric constant. The effect of backbone structure in non-aqueous solvents is not well understood, though it is intuitive that a rigid backbone may experience less swelling than a flexible backbone. While the polarity of the backbone greatly affects water uptake in aqueous solutions, the trend is not well studied and is unclear in non-aqueous solutions. In water, the highly hydrophobic backbone of Nafion exhibits less uptake than a non-fluorinated backbone such as styrene-ethylene/butylene-styrene (SEBS) triblock copolymer.[52,61] In organic solvents, such as PC, AN, and DME (dimethyloxyethane), Nafion exhibits uptake values of 65%, 19%, and 29%, respectively, while the sulfonated SEBS copolymer had no measurable solvent uptake.[61]

The IEC of the membrane also impacts solvent uptake, though the degree to which this occurs depends on the solvent dielectric constant and the salt concentration. For Li-Nafion, an increase in DME uptake only occurred at a high IEC (1.27 meq g^{-1}).[61] On the other hand, a gradual increase in PC uptake was observed with increasing IEC, with a sharp increase occurring at IECs >1.0 meq g^{-1} (Figure 14a). The lesser change in uptake for DME may be related to its low dielectric constant. For example, a high dielectric constant solvent exhibited a greater affinity for the ionic regions of sulfonated polystyrene, while a low dielectric solvent had similar affinities toward the backbone and ionic regions.[69] Thus, a change in the IEC would have a greater impact with a high dielectric solvent such as PC than the low dielectric solvent DME. Furthermore, uptake of a PPO membrane increased significantly when salt was present in an AN-based electrolyte (Figure 14b).[48] This trend is the opposite of many aqueous systems, where the presence of salt generally decreases solvent uptake (Figure 14c).[62] Furthermore, the degree to which uptake increases in the non-aqueous electrolyte solution is more pronounced at higher IEC values (~2× at 0.49 meq g^{-1} and ~3.5× at 1.03 meq g^{-1}).

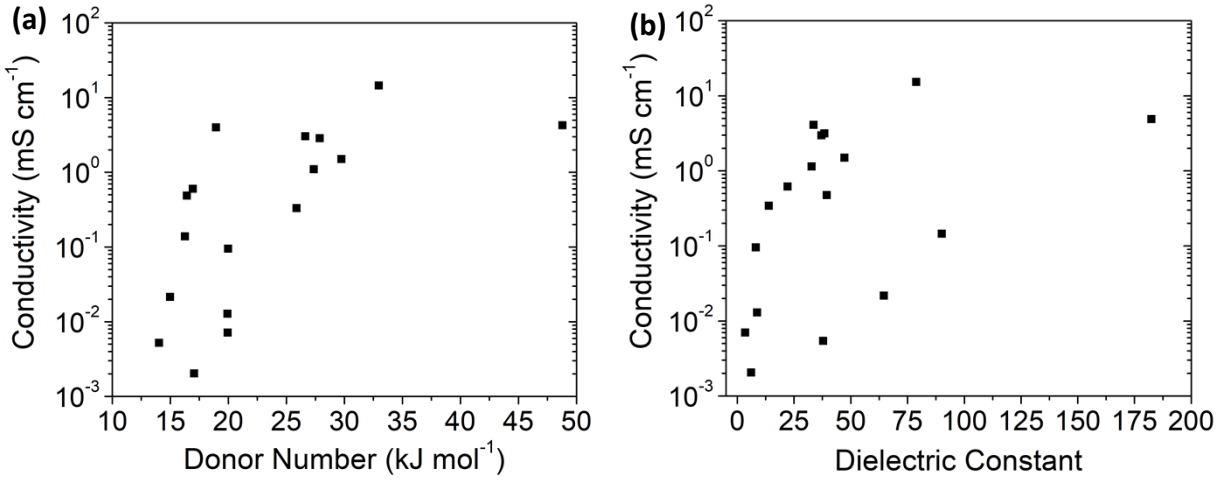

Figure 15. The conductivity of Li-Nafion as a function of solvent (a) donor number and (b) dielectric constant. Modified and reprinted with permission from Doyle et al.[56] Copyright 2001 Elsevier.

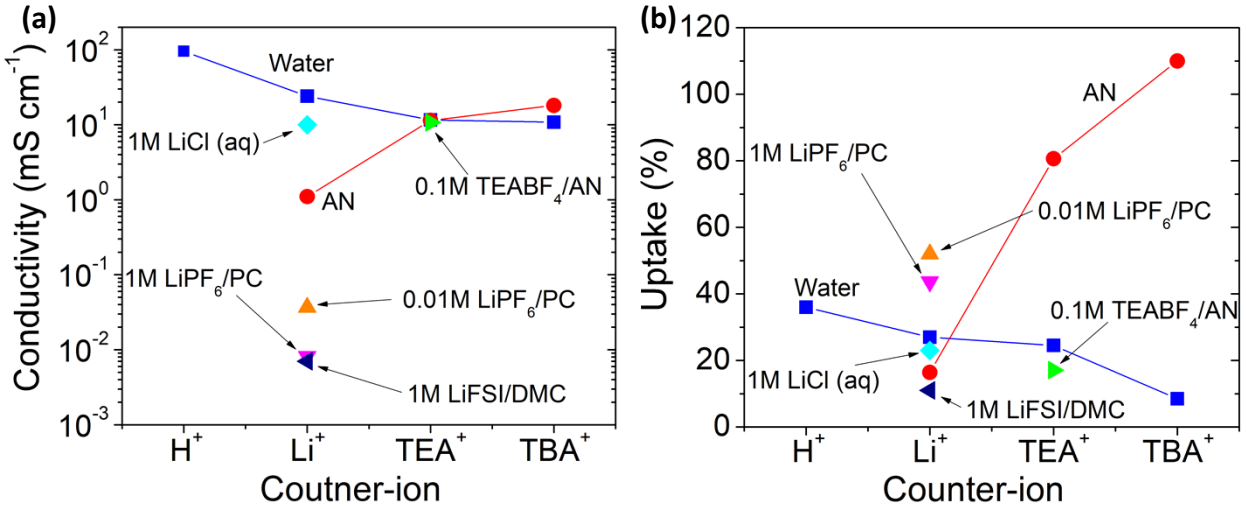

Figure 16. (a) Conductivity of Nafion or 3M perfluourinated membrane in various counter-ion forms in aqueous and non-aqueous solutions. (b) Uptake of Nafion or 3M perfluourinated membrane in various counter-ion forms in aqueous and non-aqueous solutions. AN and water data from Refs[70,71], 1M LiCl (aq) Ref[62], 0.01M and 1M $LiPF_6$ in PC Ref[72], 1M LiFSI in DMC Ref[45], 0.1M $TEABF_4$ in AN Ref[31].

Ionic Conductivity.

In non-aqueous systems, many factors contribute to the ionic conductivity of a membrane, including the solvent type, functionality of the tethered anion or cation, as well as the counter-ion. Proton transport in aqueous systems generally occurs via the Grotthus mechanism, based on H-bonding between the proton and water molecules. It is difficult to match the proton conductivity

of aqueous systems to ion conductivity in non-aqueous systems due to the lack of Grotthus-type of transport. In non-aqueous systems, ion diffusion is a much slower process; thus, developing clear correlations between membrane conductivity, solvent type, and other factors is crucial for improving the entire cell performance in NARFBs.

In general, membrane conductivity in non-aqueous solvents increases with the solvent's donor number and dielectric constant (Figure 15a and 15b). Li-Nafion has a Li^+ conductivity of 5.4×10^{-3} mS cm^{-1} in AN [56,73,74] and 2.2×10^{-2} mS cm^{-1} in PC.[56,73,74] In contrast, in water, Li^+ conductivity reaches 16 mS cm^{-1}, ~two orders higher than in non-aqueous solvents.[56,62] The difference between aqueous and non-aqueous conductivity values is partially attributed to the constriction of Nafion's ionically conductive channels. In water, the pore size of Li-Nafion is estimated to be 2.9 nm,[75,76] which decreases to 0.53 nm in PC.[72] Another reason for the decrease in ionic conductivity is the poor solvation of the Li^+ cation and the perfluoro sulfonate functional group by organic solvents, causing the Li^+ to be more tightly bound to the anion.[61,77] A further decrease in Li^+ conductivity was observed in PC for more Lewis basic anions of perfluoro carboxylate and styrene sulfonate. Thus, to promote ion disassociation in organic solvents, a very weak Lewis basic anionic group, such as a sulfonylimide, is a promising route to explore for NARFBs.[61] In Li-ion batteries, the sulfonylimide functional group is proven to provide an order of magnitude increase in Li^+ conductivity due to the highly delocalized charge on the anion.[78] Another method to promote ion disassociation is the use of an organic cation instead of an alkali metal cation.

In non-aqueous solvents, organic cations demonstrate much higher ionic conductivity than Li^+.[56,70,77] The conductivity of organic cations increases with increasing size, contrary to the trend observed in aqueous systems (Figure 16a). A perfluorinated 3M membrane (similar chemical structure to Nafion) exhibits a conductivity of 2.4 mS cm^{-1} to 18.3 mS cm^{-1} in AN with an increase in cation size from tetramethylammonium (TMA) to tetrabutylammonium (TBA).[70] In this work, the 3M membrane in lithium form had a conductivity of 1.1 mS cm^{-1}, similar to some reports for Li-Nafion,[77] but also several orders of magnitude higher than values reported elsewhere for Li-Nafion.[56,73,74] The conductivity of Nafion can depend on pretreatment conditions and equilibration time, so values here are only compared within the same work. The increase in conductivity for organic cations is attributed to the weaker electrostatic interactions between the larger TBA cation and the sulfonate groups of the polymer. In addition, the membrane in TBA^+ form exhibits a higher AN uptake (127%) than when in TMA^+ (81%) and Li^+ (16.4%) forms, which also contributes to the increase in conductivity (Figure 16b).

The effect of supporting electrolyte concentration on membrane conductivity is well documented for aqueous flow batteries, where an increase in proton conductivity is observed at low acid concentrations, then steadily declines at higher acid concentrations.[71,79] Reasons behind the decline in proton conductivity include an increase in solution viscosity and dehydration of the membrane. In neutral pH aqueous electrolytes, the conductivity of Nafion 117 depends strongly on the alkali metal cation (Figure 17a).[62] Conductivity increased with increasing salt concentration for both NaCl and LiCl, though the conductivity of NaCl was higher across the concentration range

measured (0 M to 3 M). For KCl, the conductivity slightly decreased with increasing salt concentration.

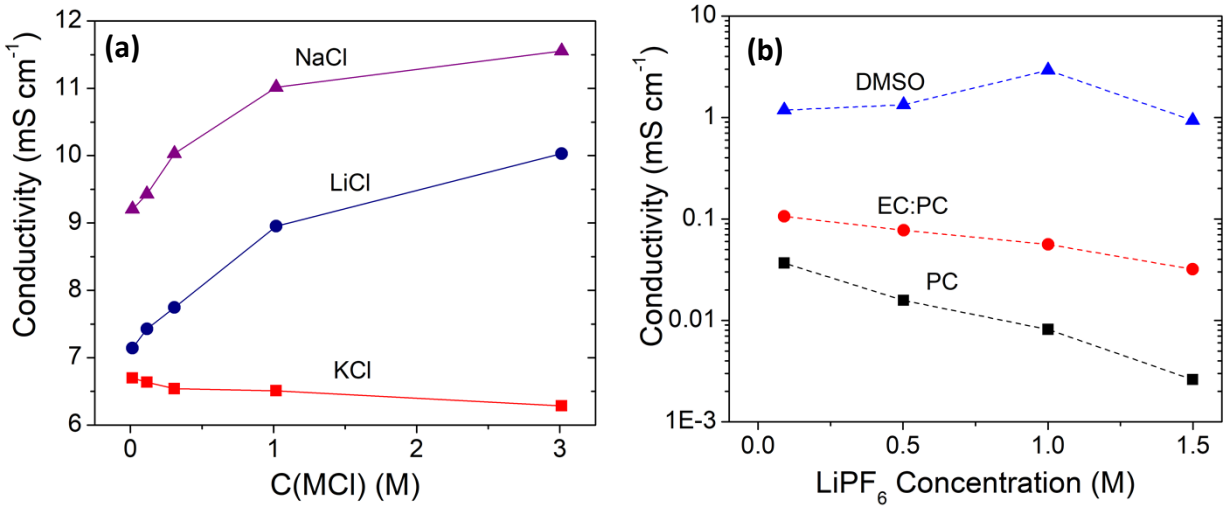

Figure 17. (a) The conductivity of Nafion-117 equilibrated in various alkali metal chloride aqueous solutions as a function of concentration. Modified and reprinted with permission from Stenina et al.[62] Copyright 2004 Elsevier. (b) The conductivity of Nafion-117 equilibrated in various organic electrolyte solutions as a function of $LiPF_6$ concentration. Modified and reprinted with permission from Su et al.[72] Copyright 2016 IOP Science.

In a non-aqueous solution, a study utilizing Nafion 117 demonstrated that a decrease in Li^+ conductivity is observed with increasing $LiPF_6$ concentration in PC. On the other hand, $LiPF_6$ concentration (0 to 1.5 M) in DMSO electrolytes had little impact on conductivity (Figure 17b).[72] In PC, the decrease in conductivity is attributed to fewer solvent molecules within the membrane as the salt concentration increases. For DMSO, the solvent uptake by Li-Nafion is considerably higher than in PC (136 wt% compared to 65 wt%).[56,72] Thus, a small decrease in the number of solvent molecules in the ion channels of Nafion soaked in $LiPF_6$ DMSO solutions has little effect on ionic conductivity. The higher viscosity of concentrated electrolytes may also play a significant role. However, there is likely a more complex set of interactions causing the decrease in conductivity that is not yet well understood. Considering that the supporting electrolyte plays such a pivotal role in NARFBs, more research into the effect of the supporting electrolyte composition on membrane conductivity is needed.

Transport Number.

Membrane selectivity for the transportation of the desired charge carrier is an important parameter for NARFB performance. The transport number is the fraction of current which arises from the movement of a given charge carrier. Typically, a high transport number for the desired ion reduces cell polarization.[80] The charge carrier can be the anion or cation depending on the redox couples utilized, but generally, an AEM is utilized for an anion charge carrier and a CEM for a cation charge carrier. From the few studies that have reported the transport number in non-aqueous

electrolytes, there appears to be a significant decrease in the transport number from aqueous to non-aqueous environments. These studies utilized the electromotive force (*emf*) method to estimate the transport number. Briefly, the cell potential is measured between compartments containing high and low concentrations of the supporting electrolyte separated by the membrane. The anion transport number ($\bar{t}_-$) through the membrane is then calculated using $V = (1 - 2\bar{t}_-)\frac{RT}{F} \ln(\frac{C_L}{C_H})$ where V is the cell potential, R is the gas constant, T is the temperature in Kelvin, F is the Faraday constant, and C_L and C_H are the low and high electrolyte concentrations, respectively.[44] While relatively dilute solutions are generally utilized to limit the impact of the activity of the electrolyte solution, studies in aqueous systems suggest that the contribution of the non-ideal thermodynamic portion may be significant in certain cases.[81] This is especially true in situations where the ion activity coefficient of the solution increases with increasing electrolyte concentration and needs to be considered for non-aqueous systems. Furthermore, developing methods to accurately determine the ion transport number in more concentrated solutions, such as those utilized in NARFBs, would provide additional insight into improving membrane performance in non-aqueous electrolytes.

Kim et al. measured the BF_4^- anion transport through two AEMs in PC and found that both exhibited a decrease in the anion transport number (0.79 and 0.87) from the Cl^- transport number in water (0.96 for both membranes).[44] Shin et al. observed an even more drastic decrease in the anion transport number of several membranes.[42] The PGMA and P4VP crosslinked membranes containing a PVDF/Si support demonstrated Cl^- transport numbers of 0.96 in aqueous solution, consistent with other reports of aqueous transport numbers.[62] [82] When immersed in a dilute 0.05 M $TEABF_4$ AN solution, the anion transport number decreased to 0.36 for the PGMA and 0.64 for the P4VP membranes. The commercial AEM, Neospeta AHA, exhibited an anion transport number of 0.98 in an aqueous electrolyte and 0.80 in the non-aqueous electrolyte 0.05 M $TEABF_4$ in AN.[42]

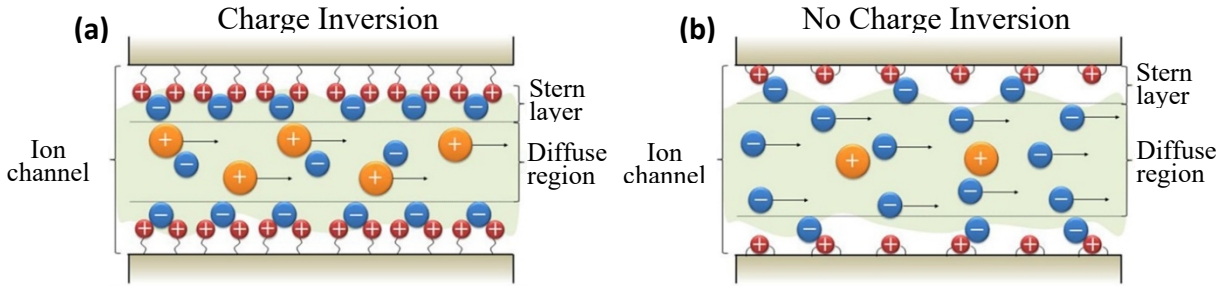

Figure 18. Schematic of ion transport through a membrane (a) with charge inversion (poly(glycidyl methacrylate) (PGMA)) and (b) without charge inversion (poly(4-vinyl pyridine) (P4VP)). Modified and reprinted with permission from Shin et al.[42] Copyright 2015 Elsevier.

A decrease in transport number could be partially due to the difference in the salts utilized. Stienna et al. demonstrated that the cation transference number is relatively size-dependent in 1M aqueous

solutions of NaCl, LiCl, and KCl.[62] The transport numbers of Li^+ and Na^+ were very similar at 0.96 and 0.97, respectively, while the transport number of the larger K^+ ion was 0.89. Furthermore, when the counter-ion was changed to the larger SO_4^{2-} ion, all the transport numbers remained above 0.98. However, even with variations in salt type, the transport numbers in aqueous systems remain significantly higher than that of the transport numbers in non-aqueous systems. Shin et al. attributed the low transport number of the PGMA membrane to charge inversion. The flexible cation in PGMA was proposed to be more accessible to the uptake of the BF_4^- counter-ion to form a Stern layer (a layer of ions counter to those tethered to the membrane) in comparison to the rigid aromatic cation of P4VP (Figure 18). Thus, charge inversion was prevented for the P4VP membrane, and a higher transport number was maintained. Even so, the ability of the membrane to exclude excess ions from entering is reduced in non-aqueous solvents compared to aqueous solutions. The poor exclusion of counter-ions implies that the effect of Donnan exclusion is weaker in organic solvents than in water. The membrane transport number behavior in non-aqueous systems needs to be further investigated to improve ion transport and reduce the redox species' permeability.

Permeability.

Reducing or eliminating the permeation of the redox couples through the membrane remains one of the greatest challenges for NARFBs. A high crossover rate of the redox species leads to low CE and EE.[42] The most widely studied redox couple to test membrane performance is $V(acac)_3$, which is positively and negatively charged when used as the catholyte and anolyte, respectively. The co-presence of charged and neutral species poses a problem for developing membranes for NARFB's, as many membranes are either cation or anion exchange, as discussed above. A few reports have utilized an aramid nanofiber support coated with layers of cation and anion exchange polymer to create a dual functionality membrane. The membrane exhibits one of the lowest $V(acac)_3$ permeabilities reported (7×10^{-10} cm^2 s^{-1}Table 2).[37] On the other hand, ferrocene (Fc, a smaller molecule than $V(acac)_3$) had several orders of magnitude higher permeability through the dual functionality aramid nanofiber membrane.[25,37] In addition, the neutral Fc species permeability was found to be higher than Fc^+ (1.1×10^{-7} cm^2 s^{-1} compared to 2.8×10^{-8} cm^2 s^{-1}).[25] The decrease in permeability of Fc^+ is attributed to electrostatic repulsion from the ion exchange layers in the membrane.

Maurya et al. measured $V(acac)_3$ permeability in its cationic, neutral, and anionic forms. The authors found that the permeation rate of $V(acac)_3$ increased with decreasing ionic size (ionic size: $V(acac)_3^-$ > $V(acac)_3$ > $V(acac)_3^+$) in low crosslink density/high IEC AEMs. However, the permeability of all three species was relatively constant for a high crosslink density/low IEC membrane.[36] If Donnan exclusion were the main factor in determining the permeability of a charged species, one would expect the highest IEC membrane should have the lowest permeability for $V(acac)_3^+$, as seen with AEMs in aqueous systems.[82] Furthermore, Mushtaq et al. found that the molar flux of Fc^+ was similar for an AEM (FAP-450) and CEM (Nafion) at ~5 μmol $h^{-1}\cdot cm^-$

[2].[83] These studies suggest that Donnan exclusion is not the major determining factor in redox species permeability for ion exchange membranes.

For neutral species, the polarity of the redox species and the polymer backbone correlate strongly with permeability. In a study utilizing a PPO backbone, neutral species permeability was found to occur through the PPO phase of the membrane rather than the ionic rich regions, thus largely unaffected by the membrane's IEC.[45,84] Furthermore, the transport of more polar molecules through the membrane was decreased compared to their less polar counterparts. The reduction in permeability of the more polar compounds is due to less favorable interactions with the PPO backbone. This study suggests that the permeability of redox species, especially that of neutral species, may be decoupled from membrane conductivity. Thus, careful design of backbone polarity in addition to ionic groups will be necessary for controlling redox species' permeability. Surprisingly, the permeability of neutral $V(acac)_3$ is an order of magnitude higher in Nafion than Fumasep FAP, even though both polymers have a similar perfluorinated backbone.[35,44] This discrepancy may be due to differences in membrane microstructure and/or the sidechain ionic groups.

The concentration of the supporting electrolyte also impacts the permeability of redox species. The permeability of Fc^+, Fc, and I^- decreased by 1.5 to 2 orders from a 0.01 M $LiPF_6$/ PC solution to a 1M $LiPF_6$/ PC solution.[72] The reduction in redox species permeability can be attributed to a decrease in electrolyte uptake with the 1M solution. These works demonstrate the complexity of redox species permeability through a membrane in non-aqueous systems. Systematic studies of permeability through polymers of varying polarities with different ionic groups are necessary. In this manner, the permeability of positive, negative, and neutral redox species could be systemically studied to gain greater insight into the factors governing their permeability through a membrane. To control redox species permeability, multiple modes of exclusion may be necessary, such as combining size exclusion with Donnan exclusion (i.e., a nanoporous substrate coated with an AEM).

Design of Membranes for NARFBs

Considering the vast combination of solvents, salts, and redox species candidates for NARFBs, designing a membrane that meets all the performance requirements mentioned above is a highly challenging task. As material selection is narrowed to fewer high-performing candidates, membrane design will also be optimized for these systems. As mentioned in the previous sections, many factors contribute to the overall performance of a membrane in a non-aqueous environment, including backbone polarity, IEC, electrolyte composition, and counter-ion. The polarity and charge of the redox species and composition of the supporting electrolyte all need to be considered when designing a membrane for a NARFB. For relatively non-polar redox species, a polar backbone may be advantageous to mitigate crossover.[84] The membrane's IEC appears to have less of an impact on the permeability of redox-active species but can significantly alter the ionic conductivity of the membranes.[45] Thus, a membrane with a higher IEC may be more beneficial for

non-aqueous systems. In addition, compared to aqueous systems, increasing membrane IEC impacts uptake to a lesser extent in non-aqueous systems, especially for non-polar solvents.[61] But an upper limit often exists on the achievable IEC of a polymer membrane. This upper limit is due to ionic aggregation that causes the polymer to become brittle.[48,85] The brittleness is especially problematic for non-aqueous systems since the polymers need to be dried thoroughly before use to remove any residual moisture. Methods employed to aid in reducing the brittleness of ion exchange membranes include crosslinking, the formation of a graft or block copolymer, and polymer blending.

As with aqueous systems, controlling membrane uptake and dimensional stability are vital engineering requirements. Methods commonly employed to control membrane uptake and swelling include crosslinking,[86] copolymerization,[87,88] and the use of a support layer.[35] Crosslinking aids in reducing dimensional swelling and improves solvent resistance. Crosslinking generally reduces solvent uptake and swelling, but can also reduce the membrane's conductivity.[89] Crosslinking alone does not typically control swelling to a sufficient degree when minimal dimensional swelling is required. Another approach includes the use of block copolymers to decouple ionic conductivity and mechanical properties. A block copolymer can have 2 to 5 dissimilar blocks, consisting of ionically conductive block(s) and mechanically robust block(s). Block copolymers have been investigated for use in aqueous systems and have been adopted with varying levels of success.[87-89] For non-aqueous systems, a block copolymer would need to be designed such that the non-aqueous electrolyte has a higher affinity towards the ionic regions rather than the mechanical blocks. This approach has not been investigated for NARFBs thus far and is a pathway worth considering.

Of these methods to control uptake and dimensional stability, the use of a porous support layer, such as Celgard, is the most effective and widely used strategy for NARFB membranes thus far. Utilizing a porous support layer is effective in minimizing dimensional swelling while allowing for a reasonable electrolyte uptake. For example, Bang et al. reported the dimensional swelling of a Celgard/ Nafion composite to be less than 0.5% with an electrolyte uptake (0.1M $TEABF_4$ in AN) of 30%. In comparison, Nafion exhibited a dimensional swelling of 9.3% with a solution uptake of 17%.[31] Methods utilized to prepare composites with a porous substrate include (i) pore filling with a monomer solution,[35,44,82] followed by polymerization, (ii) dip coating in a polymer solution (provides surface coating),[43] and (iii) infiltration of a polymer solution into the porous substrate.[90] In addition to controlling dimensional swelling, the use of a composite increases the overall strength of the membrane. The ultimate tensile strength of a composite utilizing a polyolefin separator may be significantly higher (120-150 MPa) than the neat polymer membranes (9 to 30 MPa).[31,44] Notably, the tensile strength of polypropylene-based separators depends on the direction of elongation (due to the manufacturing process), with values of 100-150 MPa and 5-15 MPa for elongation along or against the casting direction, respectively.[91]

A composite system commonly utilized in aqueous systems is the use of a polytetrafluoroethylene (PTFE) or expanded PTFE (ePTFE) support matrix. A polymer solution is typically cast with the

support matrix to obtain a membrane of excellent mechanical strength. The use of ePTFE is standard for the fabrication of Nafion-based fuel cell membranes, though the use of a composite may increase membrane cost substantially. Another promising pathway for the development of membranes for NAFRB is the use of a ceramic/polymer composite. Most highly conductive ceramic separators are brittle and difficult to fabricate as thin films. A ceramic/polymer composite can offer high single-ion conductivity while maintaining flexibility, providing a mechanically stable membrane that is potentially scalable with roll-to-roll processing. Furthermore, ceramic fillers reduce uptake and swelling of the polymer component and have been shown to aid in the reduction of redox species permeability.[16,92]

Conclusions and Outlook

Long-duration electrical energy storage is expected to play a significant role in enabling the widespread penetration of renewable energy sources into the electrical grid. NARFBs are an attractive technology for such applications due to their potential for high energy density. While much research has focused on the development of redox-active species, the development of membranes for NAFRBs is a relatively recent endeavor. Progress has been made toward achieving high-performance membranes for NARFBs, with $V(acac)_3$ permeability values in the range of $\sim 10^{-10}$ cm^2 s^{-1} and reasonable room temperature conductivity (0.1 to 5.4 mS cm^{-1}). However, significant improvements still need to be made before this technology can reach the commercialization stage.

To enable economically viable NARFBs, improvements in the redox-active species, membranes, and cell performance are necessary. The US DOE's recent announcement of the long duration storage shot sets an aggressive goal of reducing grid-scale storage cost by 90% within the next decade for systems delivering ≥10 hours of storage.[4] To fully utilize the benefits of a non-aqueous flow battery, a high concentration of active species (~4 M) and high operating voltage (3-4 V) are necessary.[93,94] Furthermore, an increase in cell voltage to 4.5 V may relax constraints on ASR and redox species concentrations.[94] In addition to active species concentration and cell voltage, performance metrics for a NARFB include an area specific resistance (which includes electrolyte and membrane) of under 5 Ω cm^2 [94] and a CE value higher than 99.99% for an asymmetric and 97% for a symmetric flow battery (where the same redox-active species is reduced on one side and oxidized on the other).[33] While the actual performance requirements are highly dependent upon the system specifications, these metrics provide useful targets. To predict the cost and performance of a flow battery, Crawford et al. reported a chemistry agnostic model based on inputs such as electrolyte and membrane conductivity and kinetic rate constants.[95] Such a model allows for the rapid evaluation of novel chemistries and will expedite the development of future NARFBs. To further advance NARFB technology, the following key areas need to be addressed:

1. Redox-active species. The chemical stability of active species needs to be improved to enable reliable long-term performance of a NARFB. Furthermore, anolytes and catholytes, which operate

at very negative/positive potentials, are needed for high voltage battery systems, but few redox-active species for NARFBs have been reported outside the window of 1.5-3.8 V vs. Li/Li^+. Lastly, the solubility of active materials needs to be improved to achieve high energy density. Alternatively, utilizing low molecular weight species capable of multiple electron processes can improve the gravimetric capacity and decrease the concentration required.[96,97]

2. Membrane To achieve a CE of 99.99%, a membrane needs to be highly selective with good chemical and mechanical stability. Active species permeability of $\leq 10^{-10}$ cm^2 s^{-1} is required for acceptable long-term performance. The chemical durability of membranes in non-aqueous systems is not well studied. Studying polymers with proven chemical stability in aqueous systems will provide benchmark values for understanding stability in a non-aqueous environment. In particular, polymers containing only hydrocarbons in the backbone have proven to be more stable in strongly basic conditions and against radical species.[50,63,98,99] The target ASR of the membrane is ≤ 2.3 Ω cm^2.[33,100] To achieve this goal, a highly conductive thin membrane is required, where for example, a 30 μm membrane needs to have a conductivity of 1.3 mS cm^{-1} to meet the ASR target. Furthermore, solvent uptake by the membrane needs to be minimized to maintain high selectivity and good mechanical properties. Celgard-based composite membranes are among the most common and effective materials reported to control swelling thus far. However, such composites are often limited to operating at low current densities (0.5 to 2 mA cm^{-2}),[35,44] and delamination of the composite is a concern during long-term operation.[48] Nanoporous membranes (pore size of 0.1-1 nm) have also been proposed as a possible candidate for NARFB separators.[33] Overall, systematic studies are necessary to develop structure-property correlations for non-aqueous electrolytes. To achieve the desired properties, a NARFB membrane will likely require a combination of a support matrix and a high-performance ion exchange polymer.

3. Cell design A reduction in electrolyte resistance is also needed to improve EE and VE of NARFBs. In addition to improving electrolyte conductivity, a reduction in the inter-electrode gap and the use of thin porous electrodes will reduce the ionic resistance of the electrolyte in the pores.[7,100] Ultimately, the optimal electrode thickness/porosity will depend on many factors, including the specific conductivity of the electrolyte, reaction kinetic parameters, redox species concentration, etc. The adoption of cell designs from well-developed aqueous systems, such as utilizing a membrane electrode assembly, may provide a route for performance improvements of NARFBs.

NARFBs represent a promising energy storage option for grid applications, but these systems still require much research and optimization to become economically viable. Continued study on all components of a NARFB is necessary, and the membrane, as a key enabler of the technology, requires significant improvements in durability, selectivity, and conductivity. Furthermore, targeted research on the effect of organic solvents on membrane transport will provide a deeper understanding of membrane properties in non-aqueous electrolytes. Establishing these structure-property relationships will provide design rules for high-performance NARFB membranes to accelerate system development and deployment.

Acknowledgments
This work is funded by Dr. Imre Gyuk, Energy Storage Program, Office of Electricity, Department of Energy.
ML also acknowledges support from the UTK Science Alliance GATE fellowship.

Author Contributions
ML wrote the majority manuscript under the guidance of TS. LT, ES, and GY wrote sections of the manuscript under the guidance of JN. JN and TS provided overall direction and supervision.

CONFLICTS OF INTEREST
There are no conflicts of interest to declare.

References

1. Veum, K., and Bauknecht, D. (2019). How to reach the EU renewables target by 2030? An analysis of the governance framework. Energy Policy *127*, 299-307.
2. Wang, T., Jiang, Z., Zhao, B., Gu, Y., Liou, K.-N., Kalandiyur, N., Zhang, D., and Zhu, Y. (2020). Health co-benefits of achieving sustainable net-zero greenhouse gas emissions in California. Nature Sustainability, 1-9.
3. Albertus, P., Manser, J.S., and Litzelman, S. (2020). Long-duration electricity storage applications, economics, and technologies. Joule *4*, 21-32.
4. Long Duration Storage Shot: An Introduction. (2021). https://www.energy.gov/sites/default/files/2021-07/Storage%20shot%20fact%20sheet_071321_%20final.pdf, Last accessed Nov 8 2021.
5. Energy Information Administration, U.S. Department of Energy, Battery Storage in the United States: An Update on Market Trends. (2020). https://www.eia.gov/analysis/studies/electricity/batterystorage/pdf/battery_storage.pdf, Last accessed Sept 14 2020.
6. Wang, Z., Yang, H., Li, Y., Wang, G., and Wang, J. (2019). Thermal runaway and fire behaviors of large-scale lithium ion batteries with different heating methods. J Hazardous Mater *379*, 120730-120738.
7. Leung, P., Shah, A., Sanz, L., Flox, C., Morante, J., Xu, Q., Mohamed, M., de León, C.P., and Walsh, F. (2017). Recent developments in organic redox flow batteries: a critical review. J Power Sources *360*, 243-283.
8. Chen, R. (2019). Toward High‐Voltage, Energy‐Dense, and Durable Aqueous Organic Redox Flow Batteries: Role of the Supporting Electrolytes. Chemelectrochem *6*, 603-612.
9. Self, E.C., Delnick, F.M., Ruther, R.E., Allu, S., and Nanda, J. (2019). High-Capacity Organic Radical Mediated Phosphorus Anode for Sodium-Based Redox Flow Batteries. ACS Energy Lett *4*, 2593-2600. 10.1021/acsenergylett.9b01744.
10. Akhil, A.A., Huff, G., Currier, A.B., Kaun, B.C., Rastler, D.M., Chen, S.B., Cotter, A.L., Bradshaw, D.T., and Gauntlett, W.D. (2015). DOE/EPRI Electricity Storage Handbook in Collaboration with NRECA. https://www.sandia.gov/ess-ssl/publications/SAND2015-1002.pdf, Last accessed Feb 24 2022.
11. Shin, S.-H., Yun, S.-H., and Moon, S.-H. (2013). A review of current developments in non-aqueous redox flow batteries: characterization of their membranes for design perspective. RSC Adv *3*, 9095-9116.
12. Yuan, J., Pan, Z.-Z., Jin, Y., Qiu, Q., Zhang, C., Zhao, Y., and Li, Y. (2021). Membranes in non-aqueous redox flow battery: A review. J Power Sources *500*, 229983-230002.
13. Gong, K., Fang, Q., Gu, S., Li, S.F.Y., and Yan, Y. (2015). Nonaqueous redox-flow batteries: organic solvents, supporting electrolytes, and redox pairs. Energ Environ Sci *8*, 3515-3530.
14. Suttil, J., Kucharyson, J., Escalante-Garcia, I., Cabrera, P., James, B., Savinell, R., Sanford, M., and Thompson, L. (2015). Metal acetylacetonate complexes for high energy density non-aqueous redox flow batteries. J Mater Chem A *3*, 7929-7938.
15. Wei, X., Cosimbescu, L., Xu, W., Hu, J.Z., Vijayakumar, M., Feng, J., Hu, M.Y., Deng, X., Xiao, J., and Liu, J. (2015). Towards high‐performance nonaqueous redox flow electrolyte via ionic modification of active species. Adv Energy Mater *5*, 1400678-1400685.

16. Bamgbopa, M.O., Shao-Horn, Y., and Almheiri, S. (2017). The potential of non-aqueous redox flow batteries as fast-charging capable energy storage solutions: demonstration with an iron–chromium acetylacetonate chemistry. J Mater Chem A *5*, 13457-13468. 10.1039/C7TA02022H.
17. Wang, W., Xu, W., Cosimbescu, L., Choi, D., Li, L., and Yang, Z. (2012). Anthraquinone with tailored structure for a nonaqueous metal–organic redox flow battery. Chem Commun *48*, 6669-6671.
18. Xing, X., Huo, Y., Wang, X., Zhao, Y., and Li, Y. (2017). A benzophenone-based anolyte for high energy density all-organic redox flow battery. Int J Hydrogen Energ *42*, 17488-17494.
19. Wei, X., Duan, W., Huang, J., Zhang, L., Li, B., Reed, D., Xu, W., Sprenkle, V., and Wang, W. (2016). A high-current, stable nonaqueous organic redox flow battery. ACS Energy Lett *1*, 705-711.
20. Geysens, P., Li, Y., Vankelecom, I., Fransaer, J., and Binnemans, K. (2020). Highly Soluble 1, 4-Diaminoanthraquinone Derivative for Nonaqueous Symmetric Redox Flow Batteries. ACS Sustain Chem Eng *8*, 3832-3843.
21. Huang, J., Yang, Z., Vijayakumar, M., Duan, W., Hollas, A., Pan, B., Wang, W., Wei, X., and Zhang, L. (2018). A Two‐Electron Storage Nonaqueous Organic Redox Flow Battery. Adv Sustain Sys *2*, 1700131-1700137.
22. Park, S.-K., Shim, J., Yang, J., Shin, K.-H., Jin, C.-S., Lee, B.S., Lee, Y.-S., and Jeon, J.-D. (2015). Electrochemical properties of a non-aqueous redox battery with all-organic redox couples. Electrochem Commun *59*, 68-71.
23. Wei, X., Xu, W., Huang, J., Zhang, L., Walter, E., Lawrence, C., Vijayakumar, M., Henderson, W.A., Liu, T., and Cosimbescu, L. (2015). Radical compatibility with nonaqueous electrolytes and its impact on an all‐organic redox flow battery. Angew Chem Int Edit *54*, 8684-8687.
24. Pan, F., Yang, J., Jia, C., Li, H., and Wang, Q. (2018). Biphenyl-lithium-TEGDME solution as anolyte for high energy density non-aqueous redox flow lithium battery. J Energ Chem *27*, 1362-1368.
25. Chai, J., Lashgari, A., Cao, Z., Williams, C.K., Wang, X., Dong, J., and Jiang, J.J. (2020). PEGylation-Enabled Extended Cyclability of a Non-aqueous Redox Flow Battery. ACS Appl Mater Inter *12*, 15262-15270.
26. Sharma, S., Rathod, S., Yadav, S.P., Chakraborty, A., Shukla, A.K., Aetukuri, N., and Patil, S. (2021). Electrochemical Evaluation of Diketopyrrolopyrrole Derivatives for Non‐aqueous Redox Flow Battery. Chemistry‐A European Journal, 12172‐12180.
27. Wei, X., Xu, W., Vijayakumar, M., Cosimbescu, L., Liu, T., Sprenkle, V., and Wang, W. (2014). TEMPO‐based catholyte for high‐energy density nonaqueous redox flow batteries. Adv Mater *26*, 7649-7653.
28. Huang, J., Cheng, L., Assary, R.S., Wang, P., Xue, Z., Burrell, A.K., Curtiss, L.A., and Zhang, L. (2015). Liquid catholyte molecules for nonaqueous redox flow batteries. Adv Energy Mater *5*, 1401782-1401788.
29. Fan, L., Jia, C., Zhu, Y.G., and Wang, Q. (2017). Redox targeting of Prussian blue: toward low-cost and high energy density redox flow battery and solar rechargeable battery. ACS Energy Lett *2*, 615-621.

30. Zhou, M., Chen, Y., Zhang, Q., Xi, S., Yu, J., Du, Y., Hu, Y.S., and Wang, Q. (2019). $Na_3V_2(PO_4)_3$ as the Sole Solid Energy Storage Material for Redox Flow Sodium‐Ion Battery. Adv Energy Mater *9*, 1901188-1901197.
31. Bang, H.S., Kim, D., Hwang, S.S., and Won, J. (2016). Surface-modified porous membranes with electrospun Nafion/PVA fibres for non-aqueous redox flow battery. J Membrane Sci *514*, 186-194.
32. Sun, C.-N., Tang, Z., Belcher, C., Zawodzinski, T.A., and Fujimoto, C. (2014). Evaluation of Diels–Alder poly (phenylene) anion exchange membranes in all-vanadium redox flow batteries. Electrochem Commun *43*, 63-66.
33. Darling, R., Gallagher, K., Xie, W., Su, L., and Brushett, F. (2015). Transport property requirements for flow battery separators. J Electrochem Soc *163*, A5029-A5040.
34. Chen, L., Venkatram, S., Kim, C., Batra, R., Chandrasekaran, A., and Ramprasad, R. (2019). Electrochemical stability window of polymeric electrolytes. Chemistry of Materials *31*, 4598-4604.
35. Kim, D., Song, J., and Won, J. (2018). Structural effects of anion exchange composite membranes in non-aqueous redox flow batteries. J Membrane Sci *564*, 523-531. 10.1016/j.memsci.2018.07.061.
36. Maurya, S., Shin, S.-H., Sung, K.-W., and Moon, S.-H. (2014). Anion exchange membrane prepared from simultaneous polymerization and quaternization of 4-vinyl pyridine for non-aqueous vanadium redox flow battery applications. J Power Sources *255*, 325-334.
37. Tung, S., Fisher, S.L., Kotov, N.A., and Thompson, L.T. (2018). Nanoporous aramid nanofibre separators for nonaqueous redox flow batteries. Nat Commun *9*, 1-9. DOI: 10.1038/s41467-018-05752-x.
38. Park, H.B., Kamcev, J., Robeson, L.M., Elimelech, M., and Freeman, B.D. (2017). Maximizing the right stuff: The trade-off between membrane permeability and selectivity. Science *356*, 1137-1147.
39. Florjańczyk, Z., Zygadło-Monikowska, E., Affek, A., Tomaszewska, A., Łasińska, A., Marzantowicz, M., Dygas, J., and Krok, F. (2005). Polymer electrolytes based on acrylonitrile–butyl acrylate copolymers and lithium bis (trifluoromethanesulfone) imide. Solid State Ionics *176*, 2123-2128.
40. Matsumoto, M., Uno, T., Kubo, M., and Itoh, T. (2013). Polymer electrolytes based on polycarbonates and their electrochemical and thermal properties. Ionics *19*, 615-622.
41. Park, C.H., Sun, Y.-K., and Kim, D.-W. (2004). Blended polymer electrolytes based on poly (lithium 4-styrene sulfonate) for the rechargeable lithium polymer batteries. Electrochim Acta *50*, 375-378.
42. Shin, S.-H., Kim, Y., Yun, S.-H., Maurya, S., and Moon, S.-H. (2015). Influence of membrane structure on the operating current densities of non-aqueous redox flow batteries: Organic–inorganic composite membranes based on a semi-interpenetrating polymer network. J Power Sources *296*, 245-254.
43. Jung, J., Won, J., and Hwang, S.S. (2020). Highly selective composite membranes using ladder-like structured polysilsesquioxane for a non-aqueous redox flow battery. J Membrane Sci *595*, 117520-117530. 10.1016/j.memsci.2019.117520.
44. Kim, D.-H., Seo, S.-J., Lee, M.-J., Park, J.-S., Moon, S.-H., Kang, Y.S., Choi, Y.-W., and Kang, M.-S. (2014). Pore-filled anion-exchange membranes for non-aqueous redox flow batteries with dual-metal-complex redox shuttles. J Membrane Sci *454*, 44-50.

45. McCormack, P.M., Luo, H., Geise, G.M., and Koenig Jr, G.M. (2020). Conductivity, permeability, and stability properties of chemically tailored poly (phenylene oxide) membranes for Li+ conductive non-aqueous redox flow battery separators. J Power Sources *460*, 228107-228117.
46. Marino, M.G., and Kreuer, K.D. (2015). Alkaline Stability of Quaternary Ammonium Cations for Alkaline Fuel Cell Membranes and Ionic Liquids. ChemSusChem *8*, 513-523. 10.1002/cssc.201403022.
47. Bamgbopa, M.O., and Almheiri, S. (2017). Influence of solvents on species crossover and capacity decay in non-aqueous vanadium redox flow batteries: Characterization of acetonitrile and 1, 3 dioxolane solvent mixture. J Power Sources *342*, 371-381.
48. Li, Y., Sniekers, J., Malaquias, J.C., Van Goethem, C., Binnemans, K., Fransaer, J., and Vankelecom, I.F. (2018). Crosslinked anion exchange membranes prepared from poly (phenylene oxide)(PPO) for non-aqueous redox flow batteries. J Power Sources *378*, 338-344.
49. Nunez, S.A., and Hickner, M.A. (2013). Quantitative H-1 NMR Analysis of Chemical Stabilities in Anion-Exchange Membranes. ACS Macro Lett *2*, 49-52. 10.1021/mz300486h.
50. Park, E.J., and Kim, Y.S. (2018). Quaternized aryl ether-free polyaromatics for alkaline membrane fuel cells: synthesis, properties, and performance - a topical review. J Mater Chem A *6*, 15456-15477. 10.1039/c8ta05428b.
51. Small, L.J., Pratt, H.D., Fujimoto, C.H., and Anderson, T.M. (2016). Diels Alder polyphenylene anion exchange membrane for nonaqueous redox flow batteries. J Electrochem Soc *163*, A5106-A5111.
52. Kraytsberg, A., and Ein-Eli, Y. (2014). Review of advanced materials for proton exchange membrane fuel cells. Energ Fuels *28*, 7303-7330. 10.1021/ef501977k.
53. Parasuraman, A., Lim, T.M., Menictas, C., and Skyllas-Kazacos, M. (2013). Review of material research and development for vanadium redox flow battery applications. Electrochim Acta *101*, 27-40.
54. Safronova, E.Y., Golubenko, D., Shevlyakova, N., D'yakova, M., Tverskoi, V., Dammak, L., Grande, D., and Yaroslavtsev, A. (2016). New cation-exchange membranes based on cross-linked sulfonated polystyrene and polyethylene for power generation systems. J Membrane Sci *515*, 196-203.
55. Wang, C., Shin, D.W., Lee, S.Y., Kang, N.R., Lee, Y.M., and Guiver, M.D. (2012). Poly (arylene ether sulfone) proton exchange membranes with flexible acid side chains. J Membrane Sci *405*, 68-78.
56. Doyle, M., Lewittes, M.E., Roelofs, M.G., Perusich, S.A., and Lowrey, R.E. (2001). Relationship between ionic conductivity of perfluorinated ionomeric membranes and nonaqueous solvent properties. J Membrane Sci *184*, 257-273.
57. Chen, J.-J.J., and Barteau, M.A. (2017). Molybdenum polyoxometalates as active species for energy storage in non-aqueous media. J Energy Stor *13*, 255-261.
58. Karabelli, D., Lepretre, J.-C., Alloin, F., and Sanchez, J.-Y. (2011). Poly (vinylidene fluoride)-based macroporous separators for supercapacitors. Electrochim Acta *57*, 98-103.
59. Shinkle, A.A., Pomaville, T.J., Sleightholme, A.E., Thompson, L.T., and Monroe, C.W. (2014). Solvents and supporting electrolytes for vanadium acetylacetonate flow batteries. J Power Sources *248*, 1299-1305.

60. Gebel, G., Aldebert, P., and Pineri, M. (1993). Swelling study of perfluorosulphonated ionomer membranes. Polymer *34*, 333-339.
61. Doyle, M., Lewittes, M.E., Roelofs, M.G., and Perusich, S.A. (2001). Ionic conductivity of nonaqueous solvent-swollen ionomer membranes based on fluorosulfonate, fluorocarboxylate, and sulfonate fixed ion groups. J Phy Chem B *105*, 9387-9394.
62. Stenina, I., Sistat, P., Rebrov, A., Pourcelly, G., and Yaroslavtsev, A. (2004). Ion mobility in Nafion-117 membranes. Desalination *170*, 49-58.
63. Lee, W.-H., Park, E.J., Han, J., Shin, D.W., Kim, Y.S., and Bae, C. (2017). Poly (terphenylene) anion exchange membranes: the effect of backbone structure on morphology and membrane property. ACS Macro Lett *6*, 566-570. 10.1021/acsmacrolett.7b00148.
64. Chen, W.T., Mandal, M., Huang, G., Wu, X.M., He, G.H., and Kohl, P.A. (2019). Highly Conducting Anion-Exchange Membranes Based on Cross-Linked Poly(norbornene): Ring Opening Metathesis Polymerization. ACS Appl Energ Mater *2*, 2458-2468. 10.1021/acsaem.8b02052.
65. Jeon, J.Y., Park, S., Han, J., Maurya, S., Mohanty, A.D., Tian, D., Saikia, N., Hickner, M.A., Ryu, C.Y., Tuckerman, M.E., et al. (2019). Synthesis of Aromatic Anion Exchange Membranes by Friedel-Crafts Bromoalkylation and Cross-Linking of Polystyrene Block Copolymers. Macromolecules *52*, 2139-2147. 10.1021/acs.macromol.8b02355.
66. Matsushita, S., and Kim, J.-D. (2018). Organic solvent-free preparation of electrolyte membranes with high proton conductivity using aromatic hydrocarbon polymers and small cross-linker molecules. Solid State Ionics *316*, 102-109. 10.1016/j.ssi.2017.12.033.
67. Han, J., Kim, K., Kim, J., Kim, S., Choi, S.-W., Lee, H., Kim, J.-j., Kim, T.-H., Sung, Y.-E., and Lee, J.-C. (2019). Cross-linked highly sulfonated poly (arylene ether sulfone) membranes prepared by in-situ casting and thiol-ene click reaction for fuel cell application. J Membrane Sci *579*, 70-78. 10.1016/j.memsci.2019.02.048.
68. Shukla, G., and Shahi, V.K. (2018). Poly(arylene ether ketone) Copolymer Grafted with Amine Groups Containing a Long Alkyl Chain by Chloroacetylation for Improved Alkaline Stability and Conductivity of Anion Exchange Membrane. ACS Appl Energ Mater *1*, 1175-1182. 10.1021/acsaem.7b00282.
69. Weiss, R., Fitzgerald, J., and Kim, D. (1991). Viscoelastic behavior of plasticized sulfonated polystyrene ionomers. Macromolecules *24*, 1064-1070.
70. Lou, K. (2021). Characterization Techniques and Cation Exchange Membrane for Non-aqueous Redox Flow Battery. Doctorate thesis *University of Tennessee*.
71. Tang, Z., Lawton, J.S., Sun, C.-N., Chen, J., Bright, M.I., Jones, A.M., Papandrew, A.B., Fujimoto, C.H., and Zawodzinski, T.A. (2014). Characterization of sulfonated Diels-Alder poly (phenylene) membranes for electrolyte separators in vanadium redox flow batteries. J Electrochem Soc *161*, A1860-A1868.
72. Su, L., Darling, R.M., Gallagher, K.G., Xie, W., Thelen, J.L., Badel, A.F., Barton, J.L., Cheng, K.J., Balsara, N.P., and Moore, J.S. (2016). An investigation of the ionic conductivity and species crossover of lithiated nafion 117 in nonaqueous electrolytes. J Electrochem Soc *163*, A5253-A5262.
73. Sachan, S., Ray, C.A., and Perusich, S.A. (2002). Lithium ion transport through nonaqueous perfluoroionomeric membranes. Polymer Eng Sci *42*, 1469-1480.

74. Sanginov, E., Evshchik, E.Y., Kayumov, R., and Dobrovol'skii, Y.A. (2015). Lithium-ion conductivity of the Nafion membrane swollen in organic solvents. Russian J Electrochem *51*, 986-990.
75. Duan, Q., Wang, H., and Benziger, J. (2012). Transport of liquid water through Nafion membranes. J Membrane Sci *392*, 88-94.
76. Schmidt-Rohr, K., and Chen, Q. (2008). Parallel cylindrical water nanochannels in Nafion fuel-cell membranes. Nat Mater *7*, 75-83.
77. Escalante-García, I.L., Wainright, J.S., Thompson, L.T., and Savinell, R.F. (2014). Performance of a non-aqueous vanadium acetylacetonate prototype redox flow battery: examination of separators and capacity decay. J Electrochem Soc *162*, A363-A373.
78. Elmore, C.T., Seidler, M.E., Ford, H.O., Merrill, L.C., Upadhyay, S.P., Schneider, W.F., and Schaefer, J.L. (2018). Ion transport in solvent-free, crosslinked, single-ion conducting polymer electrolytes for post-lithium ion batteries. Batteries *4*, 28-45.
79. Jing, M., Wei, Z., Su, W., He, H., Fan, X., Qin, Y., Liu, J., and Yan, C. (2016). Improved electrochemical performance for vanadium flow battery by optimizing the concentration of the electrolyte. J Power Sources *324*, 215-223.
80. Li, Z., Lu, W., Zhang, N., Pan, Q., Chen, Y., Xu, G., Zeng, D., Zhang, Y., Cai, W., and Yang, M. (2018). Single ion conducting lithium sulfur polymer batteries with improved safety and stability. J Mater Chem A *6*, 14330-14338.
81. Kamcev, J., Paul, D.R., Manning, G.S., and Freeman, B.D. (2017). Accounting for frame of reference and thermodynamic non-idealities when calculating salt diffusion coefficients in ion exchange membranes. J Membrane Sci *537*, 396-406.
82. Seo, S.-J., Kim, B.-C., Sung, K.-W., Shim, J., Jeon, J.-D., Shin, K.-H., Shin, S.-H., Yun, S.-H., Lee, J.-Y., and Moon, S.-H. (2013). Electrochemical properties of pore-filled anion exchange membranes and their ionic transport phenomena for vanadium redox flow battery applications. J Membrane Sci *428*, 17-23.
83. Mushtaq, K., Lagarteira, T., Zaidi, A.A., and Mendes, A. (2021). In-situ crossover diagnostics to assess membrane efficacy for non-aqueous redox flow battery. J Energy Stor *40*, 102713-102723.
84. McCormack, P.M., Koenig Jr, G.M., and Geise, G.M. (2021). Thermodynamic Interactions as a Descriptor of Cross-Over in Nonaqueous Redox Flow Battery Membranes. ACS Appl Mater Inter *13*, 49331-49339.
85. Maier, G., and Meier-Haack, J. (2008). Sulfonated aromatic polymers for fuel cell membranes. Fuel cells II, 1-62.
86. Lehmann, M.L., Yang, G., Gilmer, D., Han, K.S., Self, E.C., Ruther, R.E., Ge, S., Li, B., Murugesan, V., Sokolov, A.P., et al. (2019). Tailored Crosslinking of Poly (Ethylene Oxide) Enables Mechanical Robustness and Improved Sodium-Ion Conductivity. Energy Stor Mater *21*, 85-96.
87. Hallinan Jr, D.T., Mullin, S.A., Stone, G.M., and Balsara, N.P. (2013). Lithium metal stability in batteries with block copolymer electrolytes. J Electrochem Soc *160*, A464-A470.
88. Truong, P.V., Shingleton, S., Kammoun, M., Black, R.L., Charendoff, M., Willis, C., Ardebili, H., and Stein, G.E. (2018). Structure and properties of sulfonated pentablock terpolymer films as a function of wet–dry cycles. Macromolecules *51*, 2203-2215.

89. Mandal, M., Huang, G., and Kohl, P.A. (2019). Highly Conductive Anion-Exchange Membranes Based on Cross-Linked Poly(norbornene): Vinyl Addition Polymerization. ACS Appl Energ Mater *2*, 2447-2457. 10.1021/acsaem.8b02051.
90. Wang, T., Wang, X., Pendse, A., Gao, Y., Wang, K., Bae, C., and Kim, S. (2021). High-efficient multifunctional electrochemical membrane for lithium polysulfide redox flow batteries. J Membrane Sci, 119539-119548.
91. Kalnaus, S., Wang, Y., and Turner, J.A. (2017). Mechanical behavior and failure mechanisms of Li-ion battery separators. J Power Sources *348*, 255-263.
92. Chen, X.C., Zhang, Y., Merrill, L.C., Soulen, C., Lehmann, M.L., Schaefer, J.L., Du, Z., Saito, T., and Dudney, N.J. (2021). Gel composite electrolyte–an effective way to utilize ceramic fillers in lithium batteries. J Mater Chem A *9*, 6555-6566.
93. Darling, R.M., Gallagher, K.G., Kowalski, J.A., Ha, S., and Brushett, F.R. (2014). Pathways to low-cost electrochemical energy storage: a comparison of aqueous and nonaqueous flow batteries. Energ Environ Sci *7*, 3459-3477.
94. Dmello, R., Milshtein, J.D., Brushett, F.R., and Smith, K.C. (2016). Cost-driven materials selection criteria for redox flow battery electrolytes. J Power Sources *330*, 261-272.
95. Crawford, A., Thomsen, E., Reed, D., Stephenson, D., Sprenkle, V., Liu, J., and Viswanathan, V. (2016). Development and validation of chemistry agnostic flow battery cost performance model and application to nonaqueous electrolyte systems. International Journal of Energy Research *40*, 1611-1623. 10.1002/er.3526.
96. Kowalski, J.A., Su, L., Milshtein, J.D., and Brushett, F.R. (2016). Recent advances in molecular engineering of redox active organic molecules for nonaqueous flow batteries. Current Opinion in Chemical Engineering *13*, 45-52.
97. Laramie, S.M., Milshtein, J.D., Breault, T.M., Brushett, F.R., and Thompson, L.T. (2016). Performance and cost characteristics of multi-electron transfer, common ion exchange non-aqueous redox flow batteries. J Power Sources *327*, 681-692.
98. Wang, J.H., Zhao, Y., Setzler, B.P., Rojas-Carbonell, S., Ben Yehuda, C., Amel, A., Page, M., Wang, L., Hu, K., Shi, L., et al. (2019). Poly(aryl piperidinium) membranes and ionomers for hydroxide exchange membrane fuel cells. Nat Energy *4*, 392-398. 10.1038/s41560-019-0372-8.
99. Bai, H., Peng, H., Xiang, Y., Zhang, J., Wang, H., Lu, S., and Zhuang, L. (2019). Poly (arylene piperidine) s with phosphoric acid doping as high temperature polymer electrolyte membrane for durable, high-performance fuel cells. J Power Sources *443*, 227219-227228. 10.1016/j.jpowsour.2019.227219.
100. Sun, C.-N., Mench, M., and Zawodzinski, T. (2017). High performance redox flow batteries: an analysis of the upper performance limits of flow batteries using non-aqueous solvents. Electrochim Acta *237*, 199-206.